THE JOURNAL OF PHYSICAL CHEMISTRY B

Article

pubs.acs.org/JPCB

Phase Behavior and Molecular Dynamics Simulation Studies of New Aqueous Two-Phase Separation Systems Induced by HEPES Buffer

Mohamed Taha, Ianatul Khoiroh, and Ming-Jer Lee*

Department of Chemical Engineering, National Taiwan University of Science and Technology, 43 Keelung Road, Section 4, Taipei 106-07, Taiwan

Supporting Information

ABSTRACT: Here, for the first time, we show that with addition of a biological buffer, 4-(2-hydroxyethyl)piperazine-1-ethanesulfonic acid (HEPES), into aqueous solutions of tetrahydrofuran (THF), 1,3-dioxolane, 1,4-dioxane, 1-propanol, 2-propanol, *tert*-butanol, acetonitrile, or acetone, the organic solvent can be excluded from water to form a new liquid phase. The phase diagrams have been determined at ambient temperature. In order to understand why and how a zwitterion solute (HEPES) induced phase separation of the investigated systems, molecular dynamics (MD) simulation studies are performed for HEPES + water + THF system. The MD simulations were conducted for the aqueous mixtures with 12 different compositions. The reliability of the simulation results of HEPES in pure water and beyond the phase separation mixtures was justified by comparing the densities obtained from MD with the experimental values. The simulation results of HEPES in pure THF and in a composition inside the phase separation region were justified qualitatively. Interestingly, all HEPES molecules entirely aggregated in pure THF. This reveals that HEPES is insoluble in pure THF, which is consistent with the experimental results. Even more interestingly, the MD simulation for the mixture with composition inside the phase separation region showed the formation of two phases. The THF molecules are squeezed out from the water network into a new liquid phase. The hydrogen bonds (HBs), HB lifetime, HB Gibbs energy (ΔG), radial distribution functions (RDFs), coordination numbers (CNs), electrostatic interactions, and the van der Waals interactions between the different species have been analyzed. Further, MD simulations for the other phase separation systems by choosing a composition inside the two liquids region for each system were also simulated. Our findings will therefore pave the way for designing new benign separation auxiliary agents.

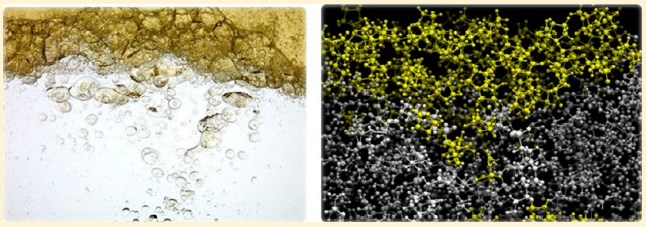

INTRODUCTION

Phase separation of organic−water solvent mixtures into two liquids with different compositions is a well-known phenomenon. The concepts that have been utilized include salting-out[1−4] and aqueous two-phase separation method,[5] each with its advantages and disadvantages. "Salting-out" refers to the separation of a water-miscible organic liquid from its aqueous solution by the addition of a salt. This method has been known for nearly a century and commonly used by biochemists in the purification of proteins.[6] The phase equilibria study for the systems containing water-miscible organic compounds, salts, and water were initiated by Frankforter and Frary,[7] who investigated methanol, ethanol, and 1-propanol with several salts. After that, the studies have been extended to various organic substances, including acetone (Frankforter and Cohen[8]), 2-propanol (Ginnings and Chen[9]), and *tert*-butanol (Ginnings and Robbins[10]). Additionally, 1,4-dioxane,[11] tetrahydrofuran (THF),[12] and acetonitile[1] were found to be salted out of water solution by several salts. However, as far as we know, no data are available for salting-out of 1,3-dioxolane from its aqueous solution.

It is noticeable that all the organic solvents in this work (THF, 1,3-dioxolane, 1,4-dioxane, 1-propanol, 2-propanol, *tert*-butanol, and acetonitile) except acetone, form azeotropes (constant boiling mixtures) with water. The existence of azeotropes is a barrier for the recovery of pure organic solvent by conventional distillation method. It has long been known that the addition of a specific material separation agent, such as a salt, into the azeotropic mixture, can change the intermolecular interactions and may break the azeotrope. However, salting-out often occurs at high salt concentrations,[13] which corrodes the equipment easily.[14,15] In analytical chemistry, salt-induced phase separation has been applied to the purification of hydrophilic proteins[16] and extraction of metalloporphyrins and metal chloride complexes.[17−19] It was found that the salting-out (or perhaps better termed "sugaring-out") separation of acetonitrile from its aqueous solution also can be achieved with high concentrations of saccharides.[20]

Aqueous two-phase systems (ATPS's) are generally formed when certain concentrations of two polymers, such as poly(ethylene glycol) (PEG) and dextran, or a polymer and salt, such as PEG and ammonium sulfate, are added to water.[21]

Received: June 5, 2012
Revised: December 16, 2012
Published: December 18, 2012

Table 1. Equilibrium Data as Weight Fraction for the Ternary System Organic Solvent (1) + HEPES (2) + Water (3) at 298.15 K under Atmospheric Pressure

solid−liq equilibrium (SLE)			liq−liq equilibrium (LLE)			solid−liq−liq equilibria (SLLE)		
w_1	w_2	w_3	w_1	w_2	w_3	w_1	w_2	w_3
			THF (1) + HEPES (2) + Water (3)					
0.0000	0.5902	0.4098	0.1328	0.3362	0.5310	0.0912	0.5441	0.3647
0.0423	0.5781	0.3796	0.2022	0.1961	0.6087	0.1198	0.5240	0.3562
			0.2668	0.1111	0.6221	0.1476	0.5082	0.3442
			0.3731	0.0674	0.5595	0.2139	0.4653	0.3208
			0.4778	0.0443	0.4779	0.2913	0.4174	0.2913
			0.5861	0.0230	0.3909	0.3881	0.3530	0.2589
			0.6937	0.0088	0.2975	0.5068	0.2758	0.2174
			0.7973	0.0028	0.1999	0.6575	0.1777	0.1648
			0.8483	0.0018	0.1499	0.7499	0.1176	0.1325
			0.8994	0.0004	0.1002	0.8386	0.0680	0.0934
			0.9494	0.0003	0.0503	0.9483	0.0014	0.0503
			1,3-Dioxolane (1) + HEPES (2) + Water (3)					
0.0000	0.5902	0.4098	0.1877	0.3744	0.4379	0.1483	0.5032	0.3485
0.0441	0.5640	0.3919	0.3197	0.2010	0.4793	0.2172	0.4542	0.3286
0.0917	0.5417	0.3666	0.4390	0.1221	0.4389	0.2942	0.4112	0.2946
			0.5523	0.0796	0.3681	0.3685	0.3633	0.2682
			0.6701	0.0420	0.2879	0.4732	0.2973	0.2295
			0.7932	0.0084	0.1984	0.6166	0.2079	0.1765
			0.8988	0.0013	0.0999	0.8122	0.0815	0.1063
						0.8700	0.0382	0.0918
			1,4-Dioxane (1) + HEPES (2) + Water (3)					
0.0000	0.5902	0.4098	0.2663	0.3341	0.3996	0.2194	0.4515	0.3291
0.0432	0.5681	0.3887	0.3958	0.2086	0.3956	0.2938	0.4126	0.2936
0.0942	0.5294	0.3764	0.5311	0.1149	0.3540	0.4112	0.3357	0.2531
0.1535	0.4886	0.3579	0.6715	0.0404	0.2881	0.5113	0.2693	0.2194
			0.7925	0.0092	0.1983	0.6516	0.1854	0.1630
			0.8986	0.0014	0.1000	0.8908	0.0100	0.0992
			1-Propanol (1) + HEPES (2) + Water (3)					
0.0000	0.5902	0.4098	0.1152	0.4243	0.4605	0.0894	0.5532	0.3574
0.0432	0.5694	0.3874	0.2368	0.2114	0.5518	0.1445	0.5189	0.3366
			0.3469	0.1331	0.5200	0.2151	0.4625	0.3224
			0.4578	0.0843	0.4579	0.2963	0.4074	0.2963
			0.5672	0.0546	0.3782	0.3927	0.3454	0.2619
			0.6828	0.0244	0.2928	0.5314	0.2407	0.2279
			0.7858	0.0173	0.1969	0.7074	0.1154	0.1772
			0.8187	0.0135	0.1678	0.7649	0.0784	0.1567
			2- Propanol (1) + HEPES (2) + Water (3)					
0.0000	0.5902	0.4098	0.1430	0.4281	0.4289	0.1209	0.5164	0.3627
0.0440	0.5613	0.3947	0.2053	0.3157	0.4790	0.1501	0.4998	0.3501
0.0928	0.5361	0.3711	0.3105	0.2238	0.4657	0.2115	0.4572	0.3313
			0.4237	0.1525	0.4238	0.3070	0.3860	0.3070
			0.5474	0.0877	0.3649	0.4053	0.3244	0.2703
			0.6693	0.0438	0.2869	0.5334	0.2380	0.2286
			0.7829	0.0214	0.1957	0.7184	0.1020	0.1796
			0.8371	0.0150	0.1479	0.8267	0.0273	0.1460
			tert-Butanol (1) + HEPES (2) + Water (3)					
0.0000	0.5902	0.4098	0.1050	0.4050	0.4900	0.0929	0.5355	0.3716
0.0438	0.5622	0.3940	0.1504	0.2481	0.6015	0.1511	0.4965	0.3524
			0.2603	0.1327	0.6070	0.2219	0.4455	0.3326
			0.3575	0.1067	0.5358	0.3016	0.3969	0.3015
			0.4704	0.0593	0.4703	0.4131	0.3115	0.2754
			0.5816	0.0308	0.3876	0.5424	0.2252	0.2324
			0.6889	0.0159	0.2952	0.7091	0.1131	0.1778
			0.7941	0.0067	0.1992	0.7913	0.0576	0.1511
			0.8368	0.0034	0.1598	0.8315	0.0273	0.1412

dx.doi.org/10.1021/jp305516g | J. Phys. Chem. B 2013, 117, 563−582

Table 1. continued

solid−liq equilibrium (SLE)			liq−liq equilibrium (LLE)			solid−liq−liq equilibria (SLLE)		
w_1	w_2	w_3	w_1	w_2	w_3	w_1	w_2	w_3
			Acetonitrile (1) + HEPES (2) + Water (3)					
0.0000	0.5902	0.4098	0.1328	0.4512	0.4160	0.1130	0.5838	0.3032
0.0420	0.5806	0.3774	0.1788	0.2866	0.5346	0.1251	0.5836	0.2913
0.0842	0.5794	0.3364	0.2441	0.1876	0.5683	0.1814	0.5465	0.2721
			0.3588	0.1030	0.5382	0.2592	0.4817	0.2591
			0.4657	0.0686	0.4657	0.3576	0.4038	0.2386
			0.5778	0.0366	0.3856	0.4696	0.3289	0.2015
			0.6904	0.0135	0.2961	0.6396	0.1997	0.1607
			0.7952	0.0050	0.1998	0.8568	0.0475	0.0957
			0.8977	0.0020	0.1003			
			Acetone (1) + HEPES (2) + Water (3)					
0.0000	0.5902	0.4098	0.1807	0.3979	0.4214	0.1522	0.4931	0.3547
0.0440	0.5600	0.3960	0.2919	0.2703	0.4378	0.2217	0.4457	0.3326
0.0955	0.5227	0.3818	0.4184	0.1632	0.4184	0.3087	0.3826	0.3087
			0.5516	0.0805	0.3679	0.4003	0.3328	0.2669
			0.6777	0.0316	0.2907	0.5370	0.2326	0.2304
			0.7921	0.0097	0.1982	0.7270	0.0911	0.1819
			0.8452	0.0058	0.1490	0.8466	0.0034	0.1500

ATPS's were for the first time reported by Berjerinck toward the end of the 19th century.[22] Such phase equilibrium systems were reinvestigated by Albertsson for the isolation and separation of plant organelles and viruses.[23] Since then, ATPS's have been increasingly used in the purification of biomolecules, such as proteins, nucleic acids, and peptides. However, the high cost of polymer and the difficulties in recycling of polymers make this concept less attractive in large-scale applications.[24]

We have observed that the addition of various zwitterionic biological buffers (TABS, MOPS, and MOBS)[25−27] into the 1,4-dioxane + water system induced phase separation with the upper phase rich in 1,4-dioxane and lower aqueous phase. Even more recently, we found another zwitterionic buffer (EPPS) induced phase separation of aqueous solutions of 1-propanol, 2-propanol, *tert*-butanol, acetonitrile, and acetone,[28,29] and this phenomenon is termed as "buffering-out". By taking the advantages of the biological buffers, i.e., inert and keep a stable pH in the physiological region of pH 6−8, the buffering-out phase separation may become better than existing methods in protein purification. The buffering-out of poly(*N*-isopropylacrylamide) (PNIPAM) from its aqueous solution by the zwitterionic biological buffers MES, MOPS, and MOPSO was also studied by our research group.[30]

This work was started to study the buffering-out of various organic solvents from their aqueous solutions using HEPES buffer. The zwitterionic buffer HEPES (HEPES ZI) has been widely used as a biological buffer within a pH range of 6.8−8.2 in cell culture medium as well as uptake and transport experiments in vitro.[31] The production of gold, silver, and platinum nanoparticles with different morphologies in HEPES solution has been reported.[32−37] It was found that HEPES acts as both reducing and stabilizing agents. As stated by Li et al.[38] the two nitrogen atoms as well as the terminal hydroxyl group of HEPES molecules are bounded to the nanoparticles surface and preventing their aggregation. An environmentally friendly hydrothermal strategy was established for the controllable synthesis of various transition metal oxide (Co_3O_4, Mn_3O_4, ZnO, and α-Fe_2O_3) nanostructures in HEPES buffer solution.[38,39] We show here several aqueous two-phase separation systems induced by HEPES buffer at 298.15 K under atmospheric pressure, namely, water + THF + HEPES; water + 1,3-dioxolane + HEPES; water + 1,4-dioxane + HEPES; water + 1-propanol + HEPES; water + 2-propanol + HEPES; water + *tert*-butanol + HEPES; water + acetonitrile + HEPES; and water + acetone + HEPES. The application of the investigated phase separation systems can be extended to the synthesis of the nanoparticles and protein crystallization at the interface of the two phases. Since there have been reports of millimeter-, micrometer-, and nano-scale particles accumulate at the interface between the two-phase systems, and a variety of interesting structures have been formed.[40−42] Moreover, protein adsorption and crystallization at the interface between two immiscible liquids is an area of considerable academic and commercial interest.[43] In order to understand the buffering-out phenomenon, molecular dynamics (MD) simulations were implemented in the present study.

EXPERIMENTAL SECTION

Materials and Methods. Purified water was taken from a NANO pure-Ultra pure water system with resistivity of 18.3 MΩ·cm. The HEPES buffer (mass fraction purity >0.995) was purchased from Sigma Chemical Co. (USA). The organic solvents *tert*-butanol (purity >0.995), 1-propanol (purity >0.99), tetrahydrofuran (THF, purity >0.9999), 1,4-dioxane (purity >0.99), acetonitrile (purity >0.99), and acetone (purity >0.9998) were purchased from Acros Organic (USA). 2-Propanol (purity >0.998) and 1,3-dioxolane (purity >0.99) were supplied by Sigma Chemical Co. (USA).

Solubility Measurements. The solubilities of HEPES in water and in aqueous organic solvent solutions beyond liquid−liquid phase splitting region, solid−liquid equilibrium data (SLE), were measured with an aid of density measurements at 298.15 K. The detailed procedure used in this work has been delineated in our earlier articles.[29,30] The densities were measured using an Anton Paar DMA 4500 digital vibrating U-tube densimeter, with automatic viscosity correction. Uncertainty of our density measurements is about $\pm 5 \times 10^{-5}$ g·cm^{-3}. The densimeter was calibrated with dry air and degassed distilled water periodically at 293.15 K. The densities

dx.doi.org/10.1021/jp305516g | J. Phys. Chem. B 2013, 117, 563−582

Table 2. Compositions of HEPES (1) + Water (2) + THF (3) Mixtures Examined by MD Simulations[a]

system	w_1	w_2	w_3	n_1	n_2	n_3	n_{total}	ρ^{exp} (kg·m^{-3})	ρ^{MD} (kg·m^{-3})	10^2 $(\Delta\rho/\rho)^b$
M1	0.0100	0.9900	0.0000	1	999	0	1000	1000.15	1001.12 ± 0.05	0.09
M2	0.0600	0.9400	0.0000	5	995	0	1000	1016.06	1022.63 ± 0.25	0.65
M3	0.1200	0.8800	0.0000	10	990	0	1000	1036.13	1046.92 ± 0.11	1.29
M4	0.1098	0.8571	0.0331	10	981	9	1000	1031.80	1044.18 ± 0.17	1.20
M5	0.1072	0.8249	0.0679	10	970	20	1000	1028.57	1039.89 ± 0.20	1.10
M6	0.1033	0.7867	0.1100	10	957	33	1000	1025.41	1033.39 ± 0.25	0.78
M7	0.1000	0.7492	0.1508	10	943	47	1000	1022.87	1023.94 ± 0.32	0.10
M8	0.1000	0.7000	0.2000	10	924	66	1000	1019.09	1013.88 ± 0.44	0.51
M9	0.0751	0.4692	0.4557	10	797	193	1000	–	–	–
M10	0.0583	0.2854	0.6563	10	629	361	1000	–	–	–
M11	0.0455	0.1448	0.8097	10	413	577	1000	–	–	–
M12	0.0310	0.0000	0.9690	10	0	990	1000	–	–	–

[a] w_1, w_2, and w_3 are the weigh fractions of HEPES, water, and THF in the mixtures, respectively. n_1, n_2, and n_3 refer to the numbers of HEPES, water, and THF molecules in an MD box, respectively. ρ^{exp} and ρ^{MD} are the experimental density and the value obtained from MD simulations, respectively. [b] $\Delta\rho/\rho = |\rho^{MD} - \rho^{exp}|/\rho_{exp}$.

are reported in Table S1 of the Supporting Information. The solubilites of HEPES in these solutions are presented in Table S2 of the Supporting Information. The uncertainty of the reported solubility limit is lower than ±0.8%.

Binodal Curves. The phase boundary curves (LLE and SLLE data) were determined by adding a buffer to aqueous solution of the organic solvent until turbidity appeared indicating the formation of a two-phase system, as described in our recent paper.[28] The uncertainty of the phase boundary determination is estimated to be ±0.0005 in mass fraction. The experimental results for the studied systems are listed in Table 1.

Computational Details. MD simulations for HEPES + water + THF systems were performed, as representatives, using GROMACS program,[44,45] version 4.0.5. All atoms were considered explicitly in a cubic box under a periodic boundary condition. Twelve composition sets (M1 to M12) were simulated in this study as given in Table 2; and the simulated systems including 1000 molecules. The compositions M1−M3 refer to HEPES in pure water. The compositions M4−M8 were chosen to simulate compositions before the phase separation region (L), while M9−M11 represent compositions inside the phase separation region (2L). The composition M12 represents HEPES in pure THF. Further, we performed MD simulations for the other phase separation systems by choosing a composition inside the (2L) region for each system because of computer time limitations. The SPC/E[46] model was applied to represent water molecules. The zwitterionic buffer (HEPES ZI) was optimized in gas phase using density functional theory (DFT) with the B3LYP method[47−50] with the standard 6-311++G(d,p) basis set as implemented in the Gaussian 09 package.[51] The buffer has been also optimized in water and THF with a polarizable continuum model (IEF-PCM) at the B3LYP/6-311++G(d,p) level. Partial atomic charges of HEPES ZI in gas phase, water, and THF were determined using the natural bond orbital (NBO) and shown in the Supporting Information (Scheme S1). The MD simulations were carried out using the OPLS-AA (Optimized Potentials for Liquid Simulations, All-Atom) force field.[52] The automated topology builder MKTOP[53] was used to extract the coordinate files of HEPES buffer, 2-propanol, and 1,4-dioxane for OPLS-AA. Then, the topologies files ware checked manually for correctness before using it. The OPLS-AA topologies, charges, structures for the organic liquids THF, 1,3-dioxolane, *tert*-butanol, acetonitrile, and acetone were taken from the Web site at http://virtualchemistry.org.[54] The topology and the charges of 1-propanol were found in the GROMACS package. The OLPS-AA charges have been assigned for 2-propanol,[52] while the charges for 1,4-dioxane was taken from ref 55. The bonding (bond stretching, angle bending, and torsion energies) and nonbonding interactions (Lennard-Jones and Coulomb energies) were calculated using the OPLS-AA force field. The chemical bonds were constrained with the LINCS algorithm. The angle bending terms were solved with a harmonic potential, while the torsion terms were modeled with a Ryckaert−Bellemans dihedral potential form. The Lennard-Jones and Coulomb potentials were applied to the atoms on different molecules or the atoms within the same molecule but separated by three covalent bonds (1−4 interactions). The cutoff for Lennard-Jones interactions was 1.4 nm, and 0.9 nm was the cutoff for the Coulomb interactions. The particle mesh Ewald (PME) algorithm with a Fourier spacing 0.125 nm and PME order 4, was used for the treatment of the Coulomb interactions.[56]

The initial configurations of the systems were prepared by randomly placing all species in the simulation box. Then, the steepest decent algorithm was performed until the maximal force on individual atoms was below 100 kJ·mol^{-1}·nm^{-1}. The cubic box was first simulated under high pressure (10 MPa) at 298.15 K for 100 ps to compress the molecules into liquid state. The systems then relaxed under atmospheric pressure (0.1 MPa) for 100 ps. All systems were stirred with *NVT* ensemble at 800 K for 200 ps. Finally, simulations were carried out with *NPT* ensemble for 10 ns at 298.15 K and 0.1 MPa for equilibration. The systems were then simulated by another 5 ns for analyses, and all coordinates were saved every 0.2 ps. Integration of Newton's equations of motion was performed with MD Leapfrog integrator[57] using a time step of 2 fs. The temperature and pressure of the simulated system were maintained constants by the Nosé−Hoover thermostat[58] and the Parrinello−Rahman barostat,[59] respectively. The molecular structures were visualized using VMD program.[60]

The MD simulations of HEPES Z1 in the gas phase were done using a stochastic dynamics (SD) integrator for 20 ns, and the gas-phase NBO charges were used. The NBO charges obtained from the optimized HEPES ZI in water were used in the MD simulation of the M1−M3 systems, while those obtained from the optimized buffer in THF were used in the

MD simulation of M12 system. We also used the former charges in the MD simulation of M4−M11 systems because of the small difference between the charges obtained from the optimized buffer in water and in THF.

The average number of hydrogen bonds $\langle N_{HB}\rangle$ per molecule for each saved frame was determined based on a geometrical criterion with a cutoff donor−acceptor (DA) distance of 0.35 nm and a cutoff donor−hydrogen−acceptor (DHA) angle of 30°,[61] because by this definition the simulated DHA angle distribution and the DA distance in water are similar to the experimental one. [61] The value of average hydrogen bond $\langle N_{HB}\rangle$ are reproduced by using the standard tool g_hbond implemented in GROMACS. The output has the form of time-resolved H-bond trajectories (values 1 or 0) for each pair that at least once is found to form an H-bond.

The radial distribution functions (RDFs) $g_{AB}(r)$ of A atom with respect to B atom were calculated by

$$4\pi r^2 g_{AB}(r) = V \sum_{i\in A}^{N_A} \sum_{j\in B}^{N_B} P(r) \quad (1)$$

where V is the volume and $P(r)$ is the probability of finding an atom B at distance r from an atom A.

RESULTS AND DISCUSSION

At ambient temperature, the studied solvents are miscible with water at any composition, giving homogeneous nonelectrolyte solution. The Gutmann's donor numbers (D_N) of THF (20.0) and 1,4-dioxane (14.8) are comparable with that of water (18.0).[62] Furthermore, Mayer−Gutmann's acceptor numbers (A_N) of the former (10.8, and 8.0, respectively) are much smaller than that of the latter (54.8).[62] Unfortunately, the corresponding parameters of 1,3-dioxolane are unavailable in the literature, but probably comparable with those of 1,4-dioxane. Thus, the cyclic ether molecules can play a role as a proton acceptor, but not a proton donor. The alcohols (as well as water) belong to class AB of the solvents;[63] the alcohols' hydroxyl group allows the formation of the hydrogen bonds with water molecules or with the molecules of alcohols. Acetonitrile, like acetone, is a dipolar, aprotic solvent, with the negative end of the dipole exposed. As a result, these compounds are completely mixed with water at any composition.

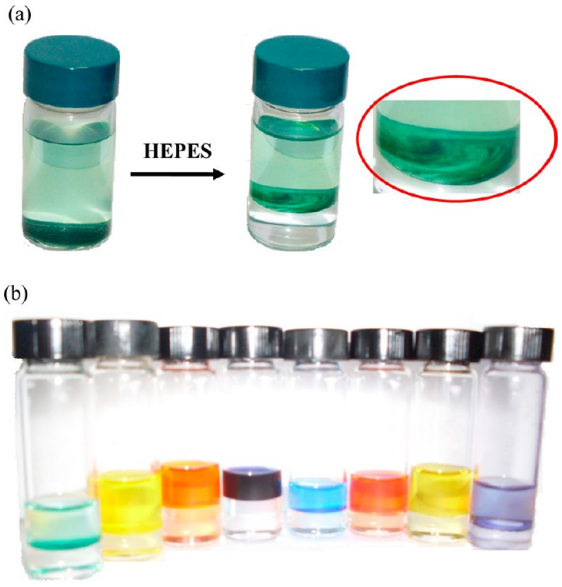

Figure 1. Photographs of buffering-out phase separations. (a) Photograph of HEPES + water + THF system; the color is due to green 9 dyestuff. (b) Photographs of HEPES-induced liquid-phase separation on aqueous solutions of THF, *tert*-butanol, 1-propanol, 2-propanol, 1,3-dioxolane, 1,4-dioxane, acetone, and aceonitrile, from left. The colors are due to green 9, yellow 119, disperse orange 25, navy SM-1P, blue 14, red 60, yellow 54, and violet 1 dyestuffs, from left.

Figure 1 shows representative HEPES-induced phase separation of THF−water mixture. At room temperature, water and THF were completely miscible, and a clear solution was obtained (Figure 1a, left). The color is due to dyestuff (green 9) dissolved in the aqueous THF solution. With addition of HEPES, the solution became turbid (cloud point) at a certain concentration of HEPES, and it gradually separated into two liquid−liquid phases with the dye concentrated in the upper THF-rich phase (Figure 1a, right). In this stable biphasic system, the upper and lower phases comprised THF-rich phase and water-rich phase, respectively, since the dye is soluble to some extent in THF and practically insoluble in water. It is noticed that dye particles assemble at the liquid−liquid interface (Figure 1a, right). In addition, the other formed two-phase systems were visualized with various disperse dyestuffs (Figure 1b). This test demonstrated the ability of two-liquid-phase systems to concentrate organic compounds in the upper phase.

The phase diagrams of the systems investigated are shown in Figures 2 and 3. In these systems we have the following conditions: two liquid substances (water and organic solvent) which are miscible in all proportions, and which in the absence of a buffer do not form phase separation; a buffer which is highly soluble in water, but practically insoluble in the organic solvent. In those graphs, the letters L and S refer to the liquid phase and the solid phase, respectively. Ignoring the vapor phase, we generally divided each phase diagram into five zones involving four different types of phase regions: a homogeneous liquid phase (L); two liquid phases (2L); one solid and two liquid phases (S + 2L), one solid and one liquid phases (S + L). Figure 2a gives a general form of the phase diagram for a ternary system of this study. The point D represents the solubility limit of the buffer in pure water (6.04 mol·kg^{-1}). From this point D a line DE (solid−liquid equilibrium, SLE, curve) runs to the point E representing the solubility limits of buffer in aqueous solutions of the organic solvent, and the organic solvent contents varying from none to the maximum possible at point E. This point E then represents the solution which is obtained by adding organic solvent to a saturated solution of the buffer in water until no more organic solvent is taken up. In general, the addition of the organic solvent reduces the solubility of the buffer in the mixture. The area ADE (S + L region) is the solid (buffer, A) in equilibrium with solutions on DE. Area EFG (2L) consists of two liquid phases only; EFG line represents the liquid−liquid equilibrium (LLE) phase boundary. Area AEG (S + 2L) is the solid (buffer, A) in equilibrium with two liquid phases (E and G); EG line is one of solid−liquid−liquid equilibrium (SLLE) phase boundaries. Area AGC (S + L) is the solid (buffer, A) in equilibrium with the organic-rich solutions containing insignificant amounts of the solid buffer, whose compositions are from G to pure organic solvent (C). The solubility limits (SLE) have been measured by densimetry method, while the binodal curves

dx.doi.org/10.1021/jp305516g | J. Phys. Chem. B 2013, 117, 563−582

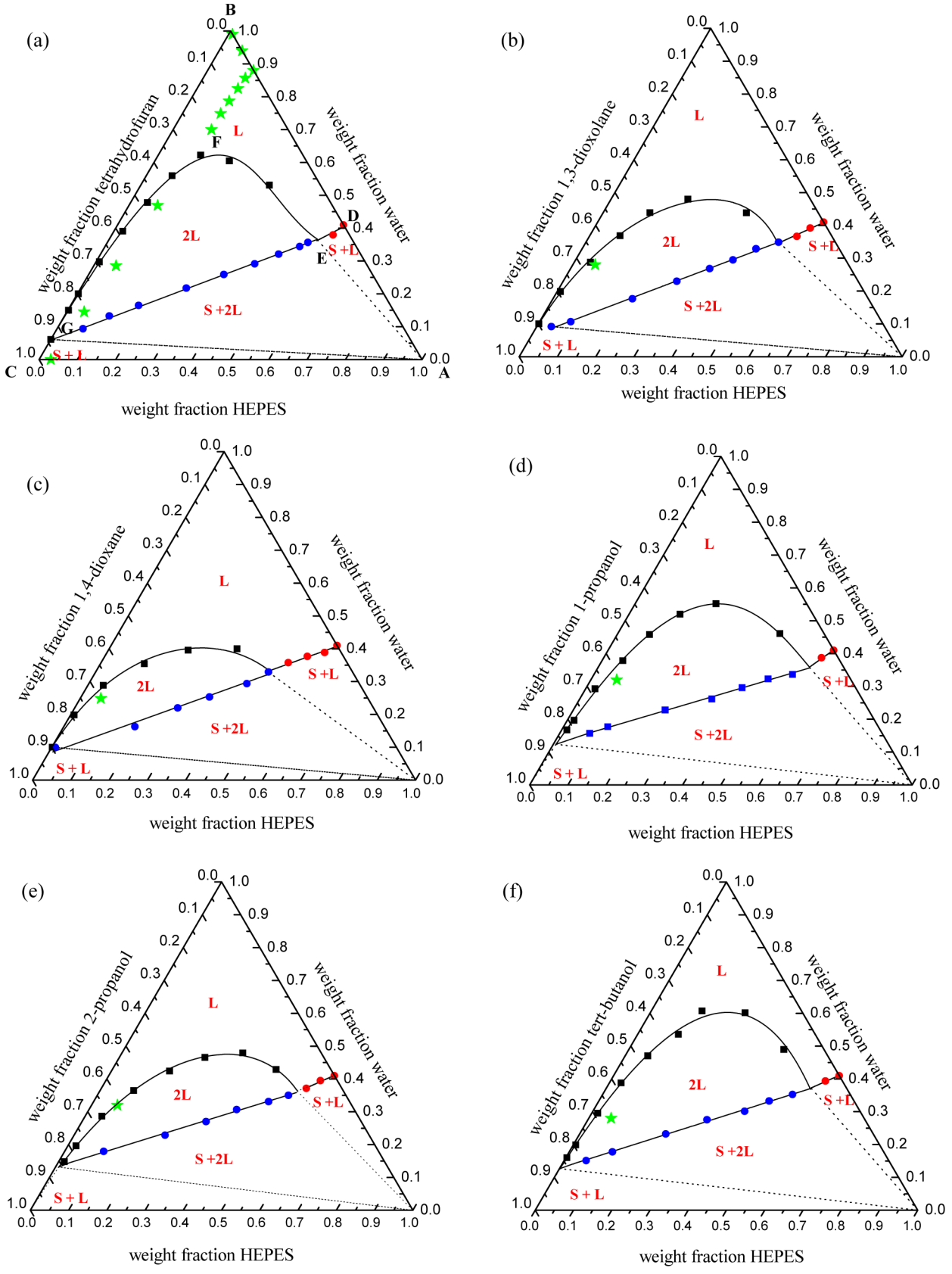

Figure 2. Phase diagrams of HEPES in aqueous solutions of THF (a), 1,3-dioxolane (b), 1,4-dioxane (c), 1-propanol (d), 2-propanol (e), and *tert*-butanol (f) at 298.15 K. The symbols red circle, blue circle, and black box represent, respectively, the solid solubility data of buffer beyond liquid phase separation (SLE), binodal data of SLLE curves, and binodal data of LLE curves. The symbol green star refers to the compositions of the MD simulations. Solid lines show the equilibrium data calculated from eq 2.

dx.doi.org/10.1021/jp305516g | *J. Phys. Chem. B* 2013, 117, 563−582

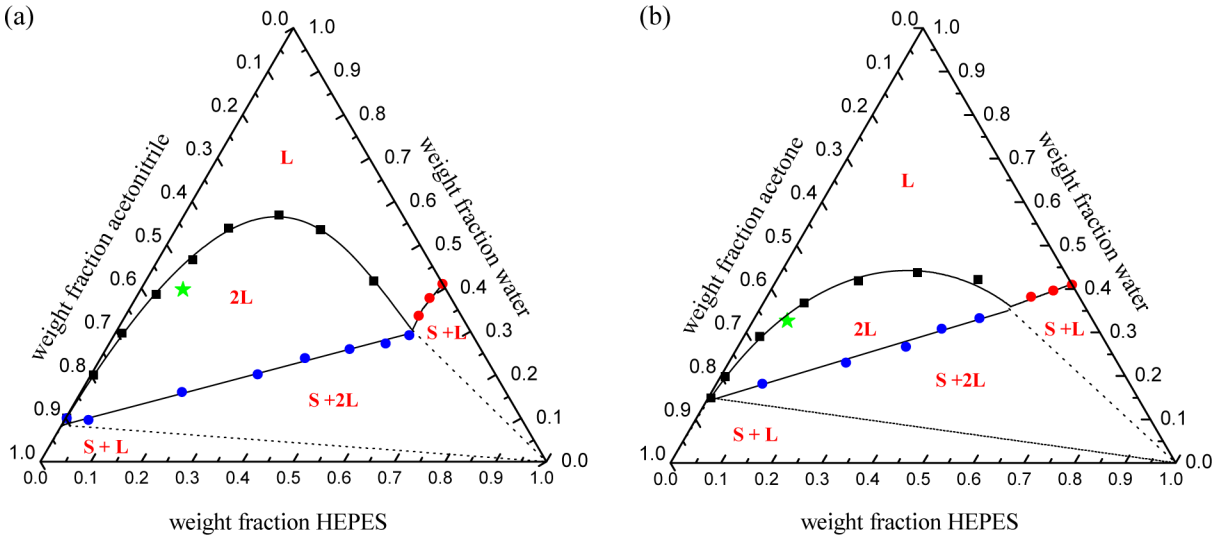

Figure 3. Phase diagrams of HEPES in aqueous solutions of acetonitrile (a) and acetone (b) at 298.15 K. The symbols and lines are as given in Figure 2 caption.

Table 3. Values of Parameters of Eq 2 for the Organic Solvent (1) + HEPES (2) + Water (3) Systems at 298.15 K

parameter	THF	1,3-dioxolane	1,4-dioxane	1-propanol	2-propanol	*tert*-butanol	acetonitrile	acetone
				Liquid−Liquid Equilibrium Data				
a	0.9705	0.946	0.9328	1.1177	1.0464	0.9911	0.9857	0.9452
b	−3.0434	−1.4827	−1.3087	−2.909	−1.8645	−2.6446	−2.5854	−1.5229
c	2.9413	0.1875	0.2414	2.1825	0.6043	1.9447	2.0532	0.4762
d	−1.4633	1.2835	0.5742	−0.4281	0.7351	−0.0065	−0.4796	0.3012
$10^2\sigma$	1.5	1.3	1.2	1.3	0.5	1.5	1.4	0.9
				Solid−Liquid Equilibrium Data[a]				
a	1.1068	1.0188	0.9084	1.4147	1.0079	1.0005	3.8248	0.9085
c	−1.861	−1.7239	−1.5342	−2.4005	−1.7107	−1.6973	−6.484	−1.5431
$10^2\ \sigma$	0.8	0.4	0.4	0.3	0.1	0.0	1.4	0.4
				Solid−Liquid−Liquid Equilibrium Data[a]				
a	0.9419	0.9372	0.9193	0.874	0.8682	0.8723	0.9167	0.8587
c	−1.566	−1.5687	−1.5301	−1.4151	−1.4396	−1.4549	−1.3641	−1.4241
$10^2\ \sigma$	0.4	0.4	1.0	0.4	0.2	0.1	0.6	0.8

[a] *b* and *d* are set to be zero.

(LLE and SLLE data) were determined using the "cloud point determination" method. It is difficult to measure accurately the solubilities of buffer from point G moving to C, because of the extremely low solubility of these buffers in this region.

The binodal LLE data at 298.15 K were fitted by the following empirical equation:

$$w_1 = a + bw_2^{0.5} + cw_2 + dw_2^3 \quad (2)$$

where w_1 and w_2 represent the weight fraction of organic solvent and HEPES buffer, respectively. The optimal values of parameters *a*, *b*, *c*, and *d* together with the corresponding standard deviations (σ) are reported in Table 3. The same equation with *b* and *d* = 0 has been used in fitting SLE and SLLE phase boundaries. In the examination of the fitted binodals with the experimental points, Figures 2 and 3 show that the empirical equation yielded a good fit to those experimental data.

In order to get an idea as to the relative efficiency in buffering-out power of the HEPES on the investigated organic solvents, we plotted the LLE binodal data in molality, as shown in Figure 4. Figure 4 reveals that tetrahydrofuran/*tert*-butanol + water systems are the easiest to be induced liquid−liquid phase splitting by HEPES among the systems investigated. The buffering out from the aqueous solutions of THF is greater than those of 1,3-dioxolane and 1,4-dioxane. When the concentration of the cyclic ether is below 6.811 mol·kg^{-1}, the buffering-out ability from 1,4-dioxane−water mixture is slightly lower than that from 1,3-dioxolane−water mixture; and when the cyclic ether concentration exceeds 6.811 mol·kg^{-1}, the buffering-out ability from 1,4-dioxane−water mixture becomes higher than that from 1,3-dioxolane−water mixture. The order for the alcohol series follows *tert*-butanol > 1-propanol > 2-propanol. As also shown in Figure 4, the buffering-out ability of acetone is higher than that of acetonitrile beyond the concentration range 6.118−9.707 mol·kg^{-1} of the organic solvent. The buffering-out efficiency of a buffer seems to be a function of its solubilities in water and in the organic solvent, which are governed by the intermolecular interactions between buffer and solvents.

In fact, several mechanisms of salt-induced phase separation of aqueous solutions of water-miscible organic solvent have been proposed on the basis of macroscopic properties, such as electrostatics,[64] thermodynamics,[65−68] and statistical mechanics.[69−71] Recently, many authors[72−76] have paid attention to

dx.doi.org/10.1021/jp305516g | J. Phys. Chem. B 2013, 117, 563−582

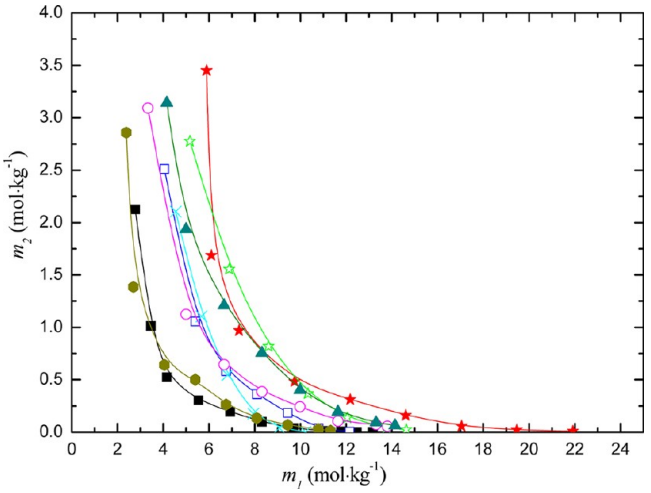

Figure 4. Buffering-out effect of HEPES on aqueous solutions of THF (■), 1,3-dioxolane (□), 1,4-dioxane (×), 1-propanol (○), 2-propanol (▲), *tert*-butanol (●), acetonitrile (★), and acetone (☆) at 298.15 K. The symbols m_1 and m_2 refer to the concentration of the organic solvent and the buffer in molality, respectively. Solid lines show only smoothness of the equilibrium data.

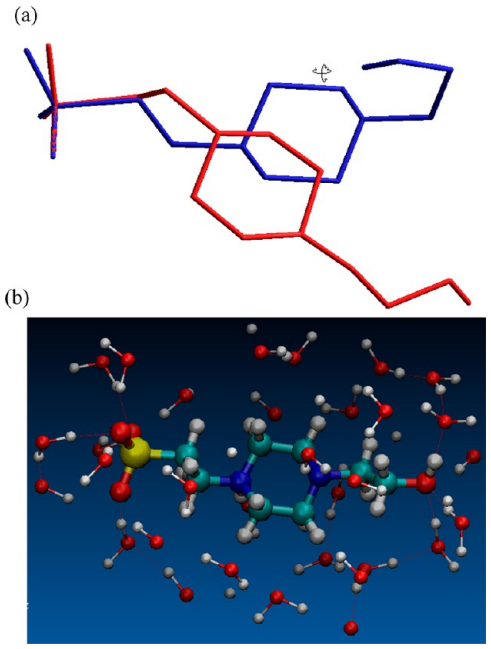

Figure 5. (a) A superposition of the HEPES in gas (blue) and water (red) molecules MD-simulated structures. The hydrogen atoms have been omitted for the sake for the clarity, except the polar hydrogens. (b) MD snapshots showing the H-bonds between HEPES and water molecules within hydrogen-bonding distances (0.35 nm), obtained from MD simulations on M1 system at 15 ns.

clarify the mechanism of salt-induced phase separation from microscopic to mesoscopic levels using SAXS and small-angle neutron scattering (SANS) techniques. The KCl + 1-propanol + water system was examined by Misawa et al.[72] and Yoshida et al.,[73] the NaCl + 1,4-dioxane + water system by Takamuku,[74] and the alkali chlorides + acetonitrile + water systems were also investigated.[75,76] Based on these investigations, mechanism of salt-induced phase separation has been proposed by the following process: first, preferential solvation of both cation and anion occurs by water molecules; second, water clusters are

Table 4. Average Number of Hydrogen Bonds $\langle N_{HB} \rangle$ Calculated from MD Simulations of HEPES (1) + Water (2) + THF (3) Mixtures

	HB per HEPES				
system[a]	HEPES–water	HEPES–HEPES	HEPES–THF	HB per THF THF–water	HB per water water–water
M1	11.94	0.06[b]	–	–	1.79
M2	11.89	0.10[c]	–	–	1.76
M3	11.67	0.15[c]	–	–	1.72
M4	11.65	0.19[c]	0.003	1.09	1.71
M5	11.60	0.20[c]	0.010	1.08	1.70
M6	11.51	0.22[c]	0.020	1.00	1.68
M7	11.40	0.25[c]	0.022	0.82	1.67
M8	11.36	0.26[c]	0.032	0.74	1.66
M9	11.16	0.29[c]	0.035	0.37	1.61
M10	11.03	0.30[c]	0.052	0.24	1.53
M11	10.64	0.38[c]	0.076	0.14	1.43
M12	–	1.56[c]	0.174	–	–

[a]The compositions of the systems M1–M12 are shown in Table 2. [b]The $\langle N_{HB} \rangle$ for the intrahydrogen bond in HEPES molecule. [c]The $\langle N_{HB} \rangle$ for the inter- and intrahydrogen bonds between HEPES molecules.

gradually evolved around both ions with increasing salt concentration, and organic molecules also aggregate to form clusters; and finally, the organic molecules are excluded from the water network, when the sizes of both water clusters and organic solvent clusters reach a macroscopic scale. On the other hand, Takamuku et al. have found recently that a non-electrolyte, *N*,*N*-dimethylformamide (DMF), induced phase separation of 1,1,1,3,3,3-hexafluoro-2-propanol (HFIP) + water mixtures;[77] and they postulated a mechanism at the molecular level based on SANS, ^{1}H and ^{13}C NMR, as well as MD simulation studies. The HFIP clusters and water clusters are formed simultaneously in the mixture; and the heterogeneity of the HFIP–water mixtures increases with increasing DMF concentration to its critical concentration for inducing the phase separation. Two methyl groups of DMF are preferentially solvated by the trifluoromethyl groups of HFIP due to the hydrophobic interaction, which enhanced the growth of HFIP clusters around DMF molecules. This generates highly hydrophobic fields in the mixtures. Additionally, water clusters form hydrophilic fields in the mixtures as well. The phase separation is occurred when the hydrophobic fields are evolved to a macroscopic scale which forces the hydrophilic fields to a new phase.[77]

In order to clarify how a zwitterion (HEPES)-induced phase separation of the investigated organics solvent + water mixtures, we performed MD simulations of HEPES buffer in the gas phase and in mixed solvents of water + THF, as representatives (Table 2). The densities obtained from the MD simulations of HEPES ZI in water (M1–M3) and in THF–water mixtures (M4–M8) at 298.15 K, as well as their comparison with experimental densities and the respective deviations, are reported in Table 2. The accuracy of the properties obtained from MD simulations depends on the reliability employed force field. As is well-known, thermodynamic properties such as heat of vaporization, free energy of solvation, heat capacity, density, viscosity, and isothermal compressibility can be used to validate the force field. We used here the experimental densities as a confirmation of the reliability of the used force field, since the other experimental properties are not available in the open

dx.doi.org/10.1021/jp305516g | J. Phys. Chem. B 2013, 117, 563–582

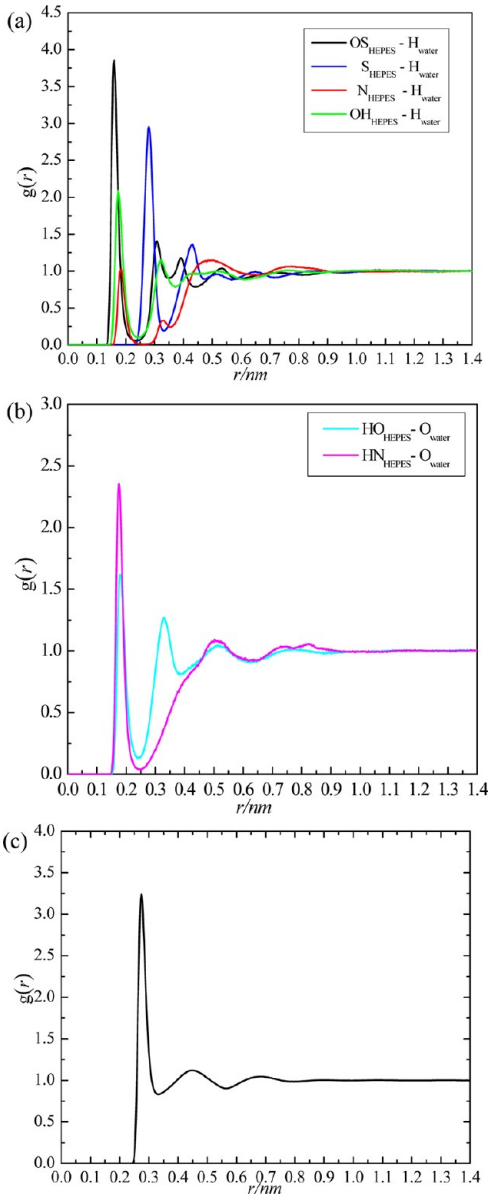

Figure 6. RDFs for the interactions of the proton acceptors (a) or donors (b) of HEPES molecules with water sites, as well as (O_{water}–O_{water}) RDF (c) those obtained from MD simulations on M3 system; (a) (OS_{HEPES}–H_{water}), (S_{HEPES}–H_{water}), (N_{HEPES}–H_{water}), and (OH_{HEPES}–H_{water}); (b) (HO_{HEPES}–O_{water}) and (HN_{HEPES}–O_{water}).

literature. Several studies have also used the liquid densities alone to estimate the precision of the force-field-based simulation.[78,79] From that table, the deviations of the simulated densities of HEPES in water (M1–M3) are ranging from 0.09 to 1.29%, while the comparison between our simulated densities of HEPES in THF–water mixtures (M4–M8) with the experimental densities showed deviations ranging from 1.20 to 0.51%. Thus, we may say that our simulated densities are agree well with the experimental values, and this leads us to be reasonably confident about our MD simulations.

It is worth mentioning that HEPES buffer has two pK_a's. The first dissociation constant (pK_{a1}) refers to the dissociation of the sulfonic group, and the second dissociation is due to dissociation of the protonated amino group (pK_{a2}). In aqueous solutions, HEPES molecule possesses, at the same time, a negatively charged sulfonic group (SO_3^-) and a positively

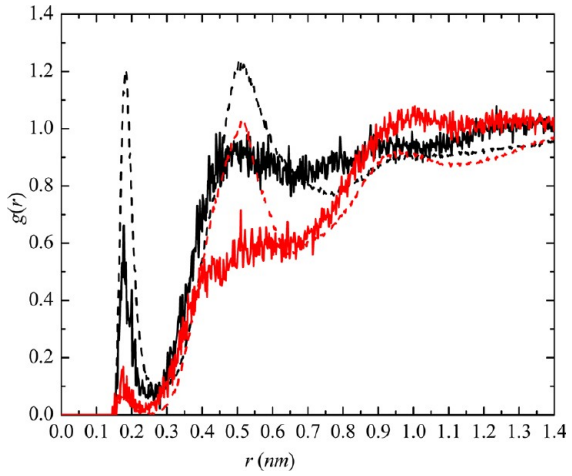

Figure 7. RDFs of (HO_{HEPES}–O_{THF}) and (HN_{HEPES}–O_{THF}) obtained from MD simulations for M4 (solid line) and M12 (dashed lines); black (HO_{HEPES}–O_{THF}) and red (HN_{HEPES}–O_{THF}).

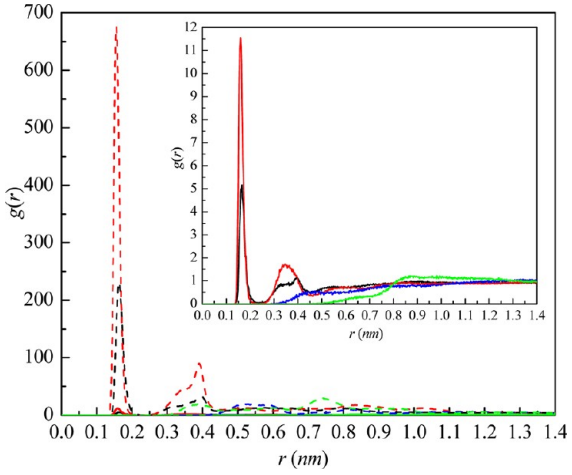

Figure 8. RDFs of HEPES–HEPES atoms obtained from MD simulations for M3 (solid line) and M12 (dashed lines); black (OS_{HEPES}–HO_{HEPES}), red (OS_{HEPES}–HN_{HEPES}), blue (HO_{HEPES}–N_{HEPES}), and green (HN_{HEPES}–NC_{HEPES}). The RDFs of HEPES–HEPES atoms obtained from MD simulations for M3 are also shown in finer scale.

Table 5. Lifetime and Gibbs Energy of Hydrogen Bonding Calculated from MD Simulations of HEPES (1) + Water (2) + THF (3) Mixtures

	lifetime (ps)		ΔG (kJ/mol)	
system[a]	HEPES–water	water–water	HEPES–water	water–water
M1	12.51	4.01	10.79	7.97
M2	13.33	4.20	10.94	8.08
M3	14.32	4.47	11.13	8.24
M4	15.04	4.78	11.25	8.41
M5	15.29	5.08	11.30	8.56
M6	15.88	5.31	11.38	8.67
M7	16.05	5.36	11.41	8.69
M8	16.88	5.50	11.54	8.76
M9	18.91	6.08	11.82	9.00
M10	23.62	7.65	12.37	9.57
M11	33.63	11.14	13.24	10.50

[a]The compositions of the systems M1–M11 are shown in Table 2.

dx.doi.org/10.1021/jp305516g | J. Phys. Chem. B 2013, 117, 563–582

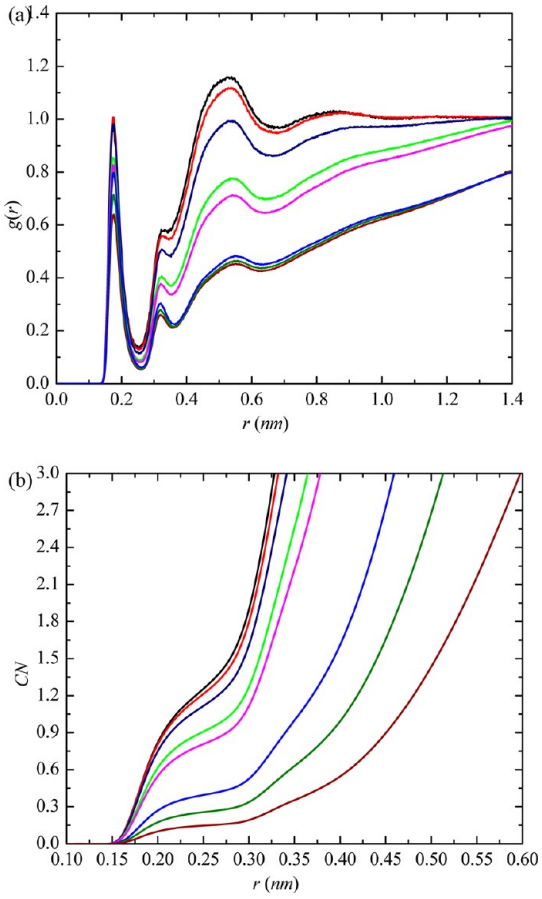

Figure 9. RDFs (a) and CNs (b) of (O_{THF}–O_{water}) obtained from MD simulations for M4 (black), M5 (red), M6 (navy), M7 (green), M8 (magenta), M9 (blue), M10 (olive), and M11 (wine).

charged amino group (NH_3^+) and becomes a zwitterion molecule. Thus, the zwitterion structure of HEPES molecules was used in the MD simulation.

Figure 5a illustrates a superposition of MD-simulated structures of HEPES molecules in the gas phase (blue) and in water medium (red). It shows that the configuration of HEPES is changed due to the interactions with water molecules. HEPES molecule has both hydrogen bond donor and acceptor sites, which provide a number of possibilities for formation of hydrogen-bonds with the solvent. The hydrogen-bond (HB) formations between the binary pairs of HEPES, water, and THF were analyzed. The average number of hydrogen bonds $\langle N_{HB} \rangle$ per molecule for each saved frame is reported in Table 4. From this table, it is apparent that the average number of H-bonds for HEPES molecule $\langle N_{HB} \rangle$ with water molecules is 11.94, and this value is slightly decreased to about 11.67 with increasing the buffer concentration from M1 to M3. In these composition sets, the HBs exist between HEPES molecules themselves are very low (0.06 at M1) and gradually increased upon increasing HEPES concentration until it reached 0.15 at M3 system. The value of $\langle N_{HB} \rangle$ at M1 (0.06) is only due to the intrahydrogen bond formation between the hydrogen atom of the hydroxyl group and nitrogen atom nearby. Thus, the observed decreasing in the H-bonds between the HEPES and water molecules at higher buffer concentration is due to the buffer–buffer interactions. Figure 5b presents MD snapshots displaying the HBs between HEPES and water molecules within hydrogen-bonding distances (0.35 nm). It is clear from this graph that significant variability of the intermolecular H-bonds between HEPES and water molecules is presented in the mixture. For instance, more than 35 water molecules exist within 0.35 nm of HEPES molecule. By examining the H-bonds formation between water and HEPES molecules, we found that the sulfonic group form at least 5 H-bonds with water molecules, while the OH group was able to

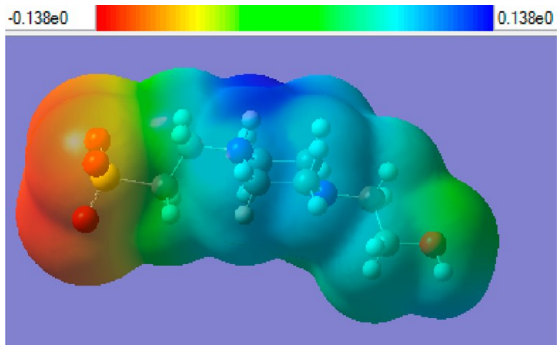

Figure 10. Electrostatic potential (ESP) of HEPES ZI in water which was mapped on an electron-density isosurface.

Table 6. Calculated Coordination Numbers for the Interactions between Selected Atoms Calculated from MD Simulations of HEPES (1) + Water (2) + THF (3) Mixtures

	HEPES–water							
system[a]	$OS_{HEPES}\cdots H_{water}$	$N_{HEPES}\cdots H_{water}$	$OH_{HEPES}\cdots H_{water}$	$S_{HEPES}\cdots H_{water}$	$HN_{HEPES}\cdots O_{water}$	$HO\cdots O_{water}$	water–water $O_{water}\cdots O_{water}$	THF–water $O_{THF}\cdots H_{water}$
M1	2.46	0.82	1.94	7.44	0.99	0.88	4.23	–
M2	2.44	0.89	1.92	7.36	0.99	0.85	4.17	–
M3	2.41	0.91	1.90	7.27	0.95	0.81	4.09	–
M4	2.41	0.91	1.86	7.26	0.93	0.80	4.04	1.31
M5	2.40	0.90	1.85	7.24	0.92	0.78	4.03	1.26
M6	2.40	0.90	1.85	7.23	0.90	0.75	4.01	1.16
M7	2.40	0.90	1.84	7.22	0.90	0.73	4.00	0.94
M8	2.40	0.83	1.82	7.22	0.90	0.73	4.00	0.83
M9	2.37	0.86	1.81	7.05	0.86	0.72	3.91	0.41
M10	2.33	0.82	1.79	7.00	0.83	0.70	3.68	0.26
M11	2.25	0.81	1.70	6.74	0.76	0.68	3.41	0.15

[a]The compositions of the systems M1 to M12 are shown in Table 2.

dx.doi.org/10.1021/jp305516g | J. Phys. Chem. B 2013, 117, 563–582

Table 7. Electrostatic (Coulomb) and the van der Waals (Lennard-Jones) Energies Obtained from MD Simulations of HEPES (1) + Water (2) + THF (3) Mixtures for the Interaction HEPES−Water, HEPES−THF, and HEPES−HEPES

	Coulomb (kJ·mol^{-1})			Lennard-Jones (kJ·mol^{-1})		
system[a]	HEPES−water	HEPES−THF	HEPES−HEPES	HEPES−water	HEPES−THF	HEPES−HEPES
M1	−689 ± 3	–	−17.4 ± 5.3	25.9 ± 0.8	–	−5.2 ± 0.1
M2	−3445 ± 14	–	−99 ± 11	146.6 ± 1.7	–	−32.1 ± 1.5
M3	−6634 ± 41	–	−276 ± 36	276.4 ± 8.3	–	−61.9 ± 4.4
M4	−6655 ± 35	−6.9 ± 0.6	−288 ± 22	290.9 ± 2.3	−25.1 ± 1.6	−65.8 ± 2.0
M5	−6676 ± 78	−14.5 ± 1.4	−343 ± 47	293.2 ± 8.4	−51.9 ± 2.5	−66.0 ± 2.4
M6	−6680 ± 54	−19.1 ± 2.8	−351 ± 28	312.0 ± 10.0	−65.0 ± 2.4	−68.3 ± 3.0
M7	−6693 ± 22	−19.6 ± 2.0	−360 ± 19	325.0 ± 5.0	−70.7 ± 5.8	−72.7 ± 2.7
M8	−6563 ± 51	−24.4 ± 2.9	−373 ± 30	329.2 ± 6.7	−86.6 ± 7.5	−74.4 ± 1.1
M9	−6407 ± 80	−25.6 ± 3.7	−407 ± 52	345.0 ± 11.0	−75.9 ± 8.5	−77.2 ± 1.4
M10	−6380 ± 92	−27.0 ± 3.0	−440 ± 51	351.0 ± 11.0	−112.9 ± 12.0	−85.2 ± 2.5
M11	−6077 ± 56	−33.7 ± 3.8	−526 ± 35	364.7 ± 6.9	−135.2 ± 8.6	−101.7 ± 6.5
M12	–	−411.9 ± 4 0.8	−1980 ± 14	–	−843.9 ± 3.5	−66.1 ± 1.9

[a]The compositions of the systems M1, M2, M3, and M4 are shown in Table 2.

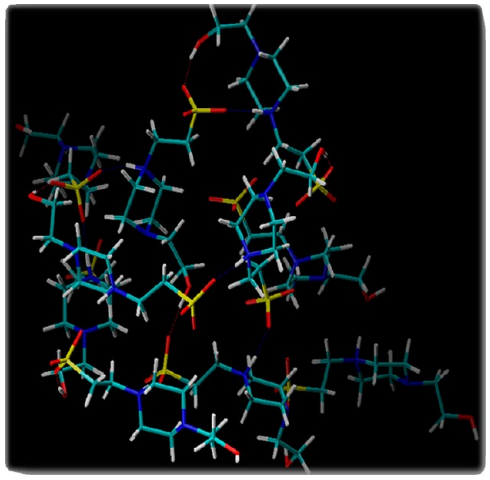

Figure 11. MD snapshot showing the aggregation of HEPES molecules in pure THF (M12 at 15 ns), as well as the HBs between HEPES molecules themselves. THF molecules have been omitted for clarity.

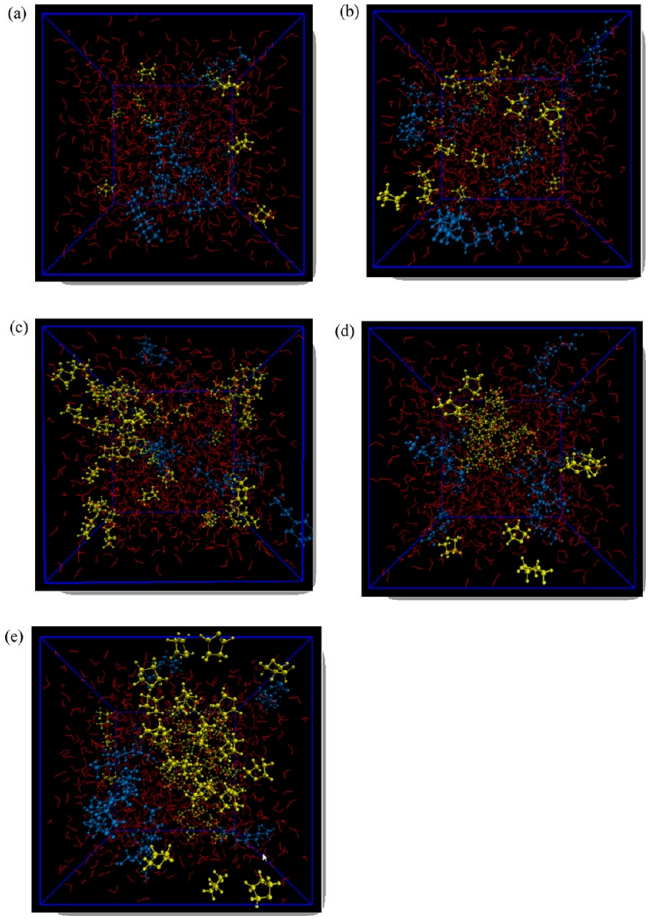

Figure 12. Snapshots displaying HEPES (blue), water (red), and THF (yellow) species obtained from MD simulations for M4 (a), M5 (b), M6 (c), M7 (d), and M8 (e) in the MD simulation box at 15 ns.

form 2 or 3 H-bonds with water molecules. In addition, the HN and N atoms are H-bonded with water, one for each atom.

Radial distribution functions (RDFs) for the acceptor and donor sites of HEPES molecule with water molecules, as well as (O_{water}−O_{water}) those obtained from MD simulation of M3 system, are shown in Figure 6. In this figure, the interactions relevant to HBs formation are observed. Through comparison of the different RDFs of the acceptor sites (Figure 6a), it appears that the dominant HBs in the mixture is of (OS_{HEPES}−H_{water}) in which one peak at 0.16 nm and three humps at 0.31, 0.39, and 0.53 nm, respectively, are observed. The peak and the first hump are attributed to the H-bonds between the sulfonic oxygen atoms and the hydrogen atoms of water according to the H-bond criteria (r < 0.35 nm, angle acceptor−H−donor below 35°), while the second and third humps arise from the nonbonding interactions between the sulfonic oxygen atoms and the other hydrogen atom of water that is not H-bonded. Bonding of the (N_{HEPES}−H_{water}) and the (OH_{HEPES}−H_{water}) types are also significant. A peak at 0.17 nm and hump at 0.32 nm for (OH_{HEPES}−H_{water}) type are raised due to the H-bond formations. The same interactions again are observed as a peak at 0.18 nm and hump at 0.33 nm for the (N_{HEPES}−H_{water}) type.

The RDFs displayed in this figure show that water molecules are more favorable to form HBs with the hydroxyl oxygen atoms (OH) than those with the amine nitrogen atoms (N). This behavior is reversed with the hydroxyl hydrogen atoms (HO) and the amine hydrogen atoms (HN); i.e., the former atoms have lower water affinity than the latter ones. The hydrogen bond distance between (HN_{HEPES}) and (O_{water}) is influenced by the positive charge of the amino group. Since the

dx.doi.org/10.1021/jp305516g | J. Phys. Chem. B 2013, 117, 563−582

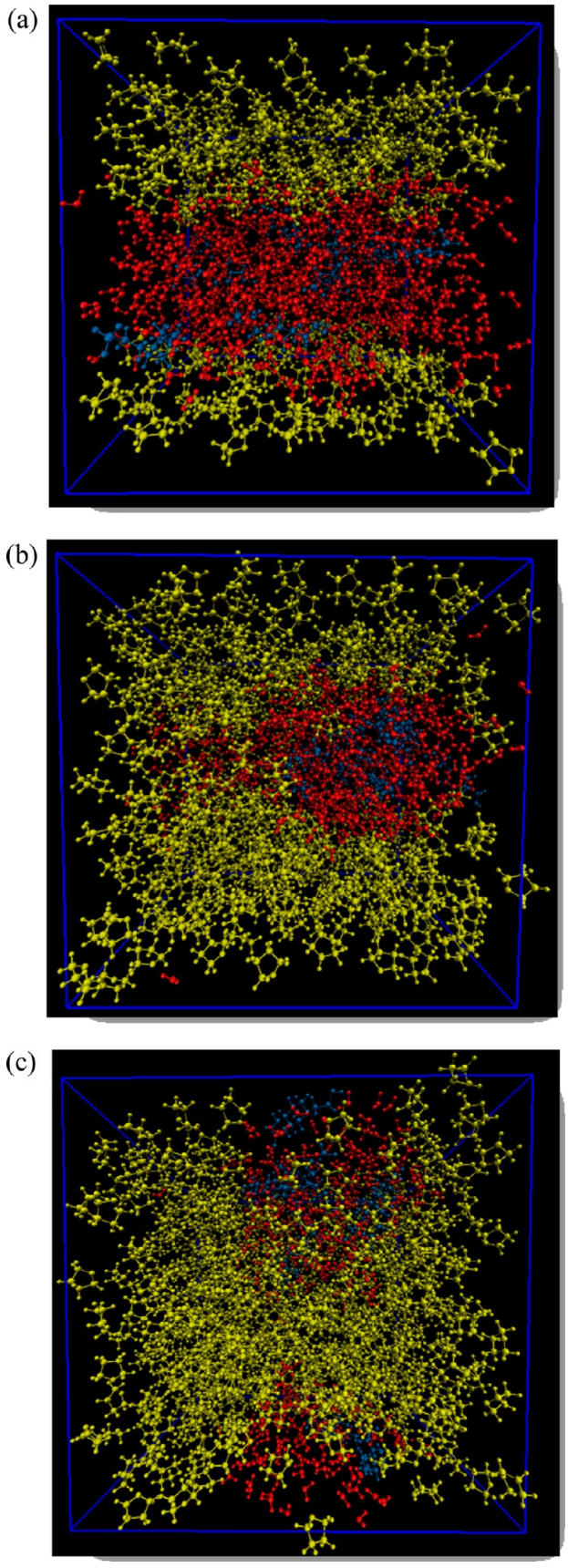

Figure 13. Snapshots displaying HEPES (blue), water (red), and THF (yellow) species obtained from MD simulations for M9 (a), M10 (b), and M11 (c) in the MD simulation box at 15 ns.

intensity peak of the (HN_{HEPES}–O_{water}) type appears at 0.17 nm, while that of the (HO_{HEPES}–O_{water}) exhibits at 0.18 nm (Figure 6b). Additionally, a hump at 0.32 nm is observed only for the latter interaction type. This hump is probably due to the nonbonding interaction between (HO_{HEPES}) and the other (O_{water}) that is hydrogen-bonded with the hydroxyl oxygen atom, but not the hydroxyl hydrogen. Interestingly, a significant peak at 0.28 nm and hump at 0.43 nm appear for the (S_{HEPES}–H_{water}) type, indicating that the sulfur atom forms H-bonds with water molecules. Indeed, the RDF results indicate that multihydration shells around HEPES are formed. All together, the RDFs and $\langle N_{HB} \rangle$ suggest that the HEPES molecules have a strong preference to be solvated by water molecules. It was observed that with increasing THF concentrations (M4 to M11), there was no significant shifting in the peaks position between HEPES and water molecules, although the relative intensities of the peaks were altered significantly (RDFs not shown).

The $\langle N_{HB} \rangle$ values between HEPES and water beyond and within the phase separation regions are slightly decreased from 11.65 to 10.64 with increasing the THF concentration from M4 to M11, respectively. This decrease in HBs shows that HEPES molecules dehydrate with increasing THF concentrations from M4 to M11. These results agree well the experimental observation in which the solubility of HEPES decreases with increase in the THF concentrations. These results are further supported by gradually increasing the $\langle N_{HB} \rangle$ between HEPES molecules from 0.19 to 1.56 with increasing the THF concentration from M4 to M12, respectively.

The HBs formation between HEPES and THF molecules are very small and insignificantly increased with increasing the THF concentration from M4 to M11(see Table 4). We can see also from Table 4 that the $\langle N_{HB} \rangle$ value between HEPES and THF is also very small in pure THF (M12), 0.174, showing the low affinity of HEPES toward THF. Furthermore, the $\langle N_{HB} \rangle$ values between THF and water molecules in the homogeneous liquid-phase region (M4–M8) are higher than those inside the phase separation region (M9–M11); i.e., with increasing THF concentration from M4 to M11 the $\langle N_{HB} \rangle$ value is sharply decreased from 1.09 to 0.14, respectively, due to the phase separation. The hydrogen atoms of the hydroxyl and the protonated amine groups of HEPES molecule can form interhydrogen bonds with the oxygen atoms of the THF molecules and the corresponding RDFs are given in Figure 7. At low THF concentration (M4), a peak at ∼0.18 nm is observed relevant to the inter-HBs formation between (HO_{HEPES})/(HN_{HEPES}) atoms and (O_{THF}) atoms. The intensity of the HO_{HEPES}–O_{THF} peak obtained from MD of M4 system is greater than that of the HN_{HEPES}–O_{THF} peak. The intensity of the former peak is increased in pure THF (M12), while the latter peak is almost constant. Further, a second peak at ∼0.5 nm appeared in pure THF for both interactions, (HO_{HEPES}–O_{THF}) and (HN_{HEPES}–O_{THF}).

Figure 8 shows the RDFs of HEPES–HEPES atoms in water (M3) and in pure THF (M12). In pure water, two strong peaks are showed for (OS_{HEPES}–HN_{HEPES}) type and (OS_{HEPES}–HO_{HEPES}) type at ∼0.16 nm due to the HBs formation, and the intensity of the former peak is greater than the latter one. The graph also shows that no HBs formation is observed for HN_{HEPES}–N_{HEPES} type or HO_{HEPES}–N_{HEPES} type in water; since no peak is shown within hydrogen-bonding distances. However, there is abroad peak starting from ca. 0.30 to 0.45 nm for HN_{HEPES}–N_{HEPES} type in pure THF. Thus, besides the

dx.doi.org/10.1021/jp305516g | J. Phys. Chem. B 2013, 117, 563–582

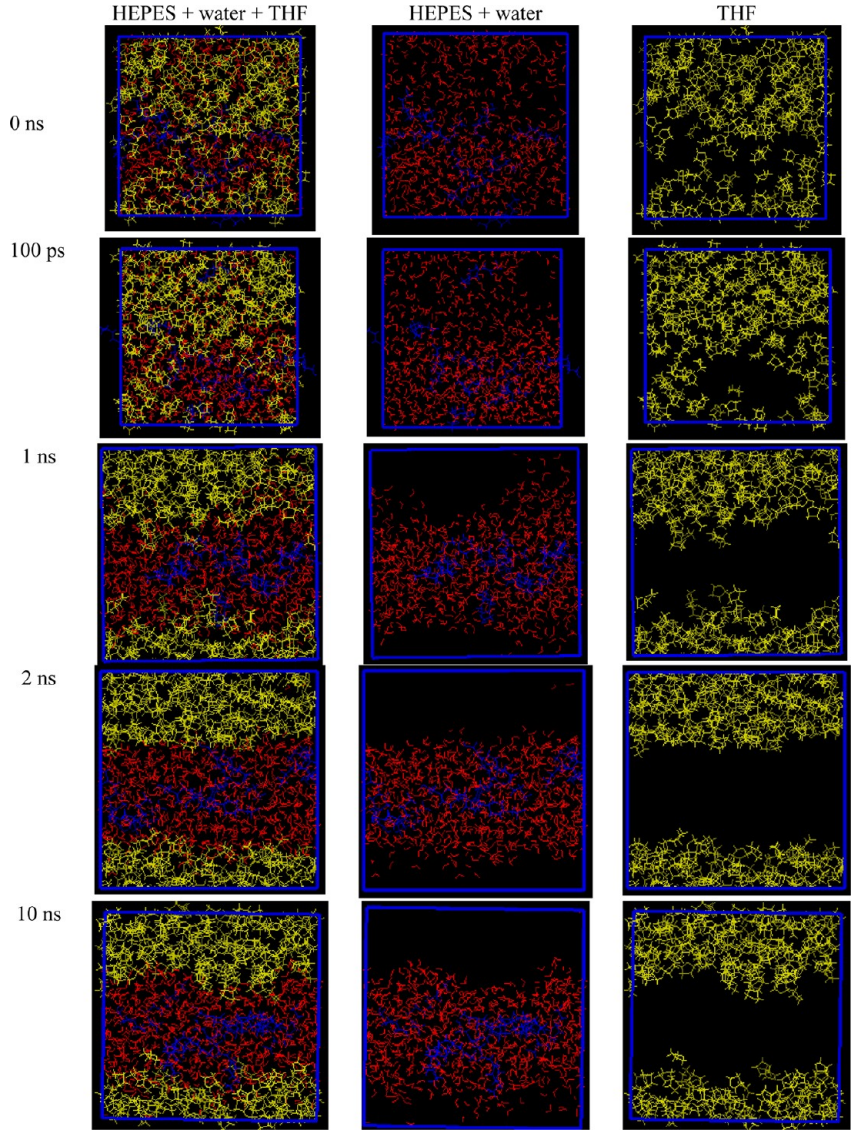

Figure 14. Snapshots displaying HEPES (blue), water (red), and THF (yellow) species obtained from MD simulations of M9 at different simulation times.

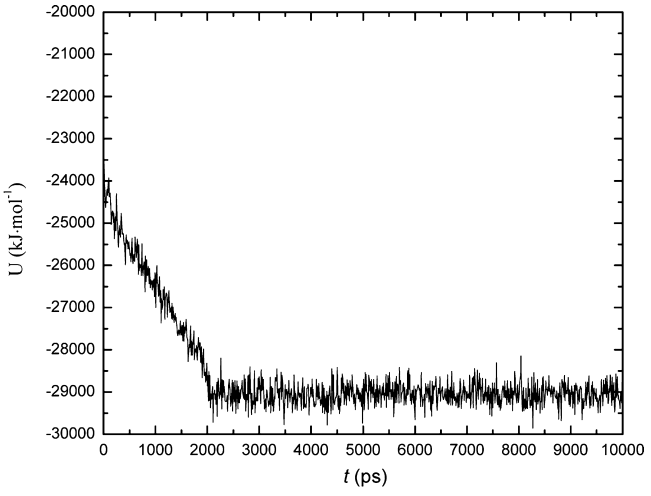

Figure 15. Potential energy (U) obtained from MD simulations of M9 as a function of time (ps).

formation of inter-HBs between the OS and HN/HO groups of HEPES molecules in pure organic solvent, other inter-HBs between the HN and N atoms can be also formed. Thus, the low solubility of HEPES molecules in pure THF is reinforced again from the high intensity of the RDF peaks due to the strong interactions between HEPES molecules themselves.

The HBs between the water molecules themselves are slightly influenced by the addition of THF (Table 4). To evaluate the strengths of the HBs of the water network, as well as between HEPES and water, we calculated the lifetimes and the Gibbs energy (ΔG) of HBs with the interrupted HB method (first-order dynamics method).[61] From the values reported in Table 5, we can conclude that the lifetime and the ΔG values have increased with increasing THF concentration, although with decrease in the corresponding $\langle N_{HB} \rangle$ values (Table 4). This shows the high water affinity of HEPES even at low water mass fractions (high THF concentrations). It is clear from the above discussion that both water and THF clusters are formed in the mixture; and the HEPES molecules are strongly solvated by water molecules. The interactions between water and THF clusters have weakened with increasing the THF

dx.doi.org/10.1021/jp305516g | J. Phys. Chem. B 2013, 117, 563−582

Table 8. Average Number of Hydrogen Bonds $\langle N_{HB} \rangle$ Calculated from MD Simulations of HEPES + Water + Organic Solvent Systems

	HB per HEPES				
$S_{organic\ solvent}$ [a]	HEPES–water	HEPES–HEPES	HEPES–ORG	HB per ORG[b] ORG–water	HB per water water–water
S_{THF}	11.03	0.30[c]	0.052	0.24	1.53
$S_{1,3\text{-dioxolane}}$	11.78	0.27[c]	0.024	0.31	1.49
$S_{1,4\text{-dioxane}}$	11.54	0.27[c]	0.020	0.29	1.50
$S_{1\text{-propanol}}$	10.01	0.46[c]	0.721	1.32	1.21
$S_{2\text{-propanol}}$	10.57	0.25[c]	0.754	1.30	1.22
$S_{tert\text{-butanol}}$	11.04	0.24[c]	0.470	1.18	1.24
$S_{acetonitrile}$	9.75	0.43[c]	0.200	0.78	1.25
$S_{acetone}$	11.25	0.28[c]	0.057	0.418	1.43

[a] S_{THF} = HEPES + water + THF system; $S_{1,3\text{-dioxolane}}$ = HEPES + water +1,3-dioxolane system; $S_{1,4\text{-dioxane}}$ = HEPES + water +1,4-dioxane system; $S_{1\text{-propanol}}$ = HEPES + water +1-propanol system; $S_{2\text{-propanol}}$ = HEPES + water +2-propanol system; $S_{tert\text{-butanol}}$ = HEPES + water + *tert*-butanol system; $S_{acetonitrile}$ = HEPES + water + acetonitrile system; and $S_{acetone}$ = HEPES + water + acetone system. The simulation box contains 10 HEPES, 629 water, and 361 organic solvent molecules. [b] ORG refers to organic solvent. [c] The $\langle N_{HB} \rangle$ for the inter and intrahydrogen bonds between HEPES molecules.

concentrations, as it appears from the $\langle N_{HB} \rangle$ between THF and water molecules. Figure 9a shows the RDF of O_{THF}–O_{water} interaction. A sharp peak with low intensity appears at 0.17 nm due to the HBs formation. In addition, a broad peak around 0.5 nm with small shoulder at 0.32 nm is also observed. It is essential to know if the coordination number (CN) and HBs are similar. The CNs were calculated for the interactions between selected atoms integrating the corresponding RDFs, and the values are summarized in Table 6. From this table, we can see that the CNs are consistent with the $\langle N_{HB} \rangle$ results. For instance, the CN values for the first peak of the O_{THF}–O_{water} interactions (Figure 9b) gradually decreased before the phase separation (M4 to M8), and then sharply decreased from M9 to M11 due to the phase separation.

The zwitterions, like electrolytes, have very large dipole moments[80−82] and interact electrostatically with solvent and other charged molecules in the solution.[83−86] The calculated dipole moment of HEPES in water, using DFT-B3LYP levels with the 6-311++G(d,p) basis set, is 23.8082 D. Further, Figure

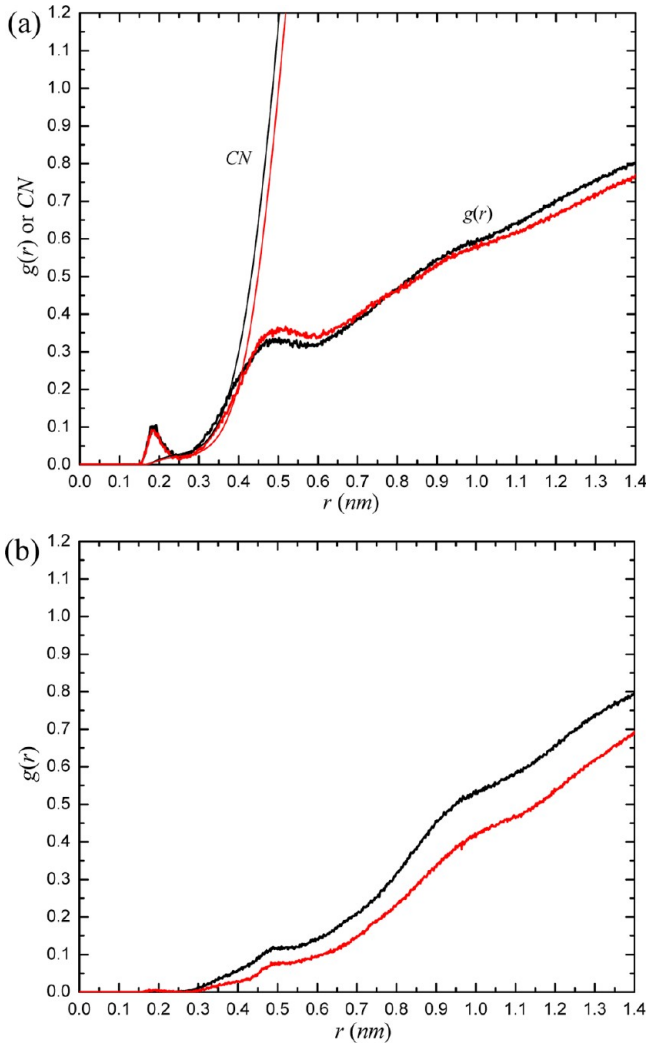

Figure 16. RDFs and CNs of (HO_{HEPES}–$O_{cyclic\ ether}$) and (HN_{HEPES}–$O_{cyclic\ ether}$) obtained from MD simulations of $S_{1,3\text{-dioxolane}}$ (black), and $S_{1,4\text{-dioxane}}$ (red) systems. The CNs for $HN_{HEPES}\cdots O_{cyclic\ ether}$ are not shown because it was not possible to identify the first peak. $S_{1,3\text{-dioxolane}}$ = HEPES + water + 1,3-dioxolane system and $S_{1,4\text{-dioxane}}$ = HEPES + water + 1,4-dioxane system.

Table 9. Electrostatic (Coulomb) and the van der Waals (Lennard-Jones) Energies Obtained from MD Simulations for the Interaction HEPES–Water, HEPES–ORG[a], and HEPES–HEPES

	Coulomb (kJ·mol^{-1})			Lennard-Jones (kJ·mol^{-1})		
$S_{organic\ solvent}$ [b]	HEPES–water	HEPES–ORG	ORG–water	HEPES–water	HEPES–ORG[b]	ORG–water
S_{THF}	−6380 ± 92	−27.0 ± 3.0	−1886 ± 12	351.0 ± 11.0	−112.9 ± 12.0	−1154.6 ± 7.4
$S_{1,3\text{-dioxolane}}$	−6931 ± 88	−52.3 ± 3.8	−2394 ± 38	402.9 ± 12.0	−148.5 ± 6.7	−1293.4 ± 10.0
$S_{1,4\text{-dioxane}}$	−6892 ± 75	−35.4 ± 3.4	−2229 ± 26	398.5 ± 8.1	−131.9 ± 5.8	−1270.4 ± 14.0
$S_{1\text{-propanol}}$	−5843 ± 61	−381.5 ± 32	−12553 ± 110	412.9 ± 4.1	−265.8 ± 5.7	−507.3 ± 5.8
$S_{2\text{-propanol}}$	−6276 ± 49	−373.5 ± 40	−12433 ± 240	467.7 ± 10.0	−302.4 ± 12.0	−629.4 ± 9.3
$S_{tert\text{-butanol}}$	−6557 ± 66	−191.3 ± 13	−11114 ± 98	453.2 ± 3.9	−220.0 ± 5.9	−588.6 ± 20
$S_{acetonitrile}$	−5555 ± 59	−310.6 ± 11	−8030 ± 39	436.7 ± 8.7	−269.4 ± 4.9	−957.9 ± 4.5
$S_{acetone}$	−6637 ± 90	−66.4 ± 3.8	−3703 ± 56	402.5 ± 5.3	−132.4 ± 4.3	−1278.6 ± 18.0

[a] ORG refers to organic solvent. [b] S_{THF} = HEPES + water + THF system; $S_{1,3\text{-dioxolane}}$ = HEPES + water +1,3-dioxolane system; $S_{1,4\text{-dioxane}}$ = HEPES + water +1,4-dioxane system; $S_{1\text{-propanol}}$ = HEPES + water +1-propanol system; $S_{2\text{-propanol}}$ = HEPES + water +2-propanol system; $S_{tert\text{-butanol}}$ = HEPES + water + *tert*-butanol system; $S_{acetonitrile}$ = HEPES + water + acetonitrile system; and $S_{acetone}$ = HEPES + water + acetone system. The simulation box contains 10 HEPES, 629 water, and 361 organic solvent molecules.

dx.doi.org/10.1021/jp305516g | J. Phys. Chem. B 2013, 117, 563−582

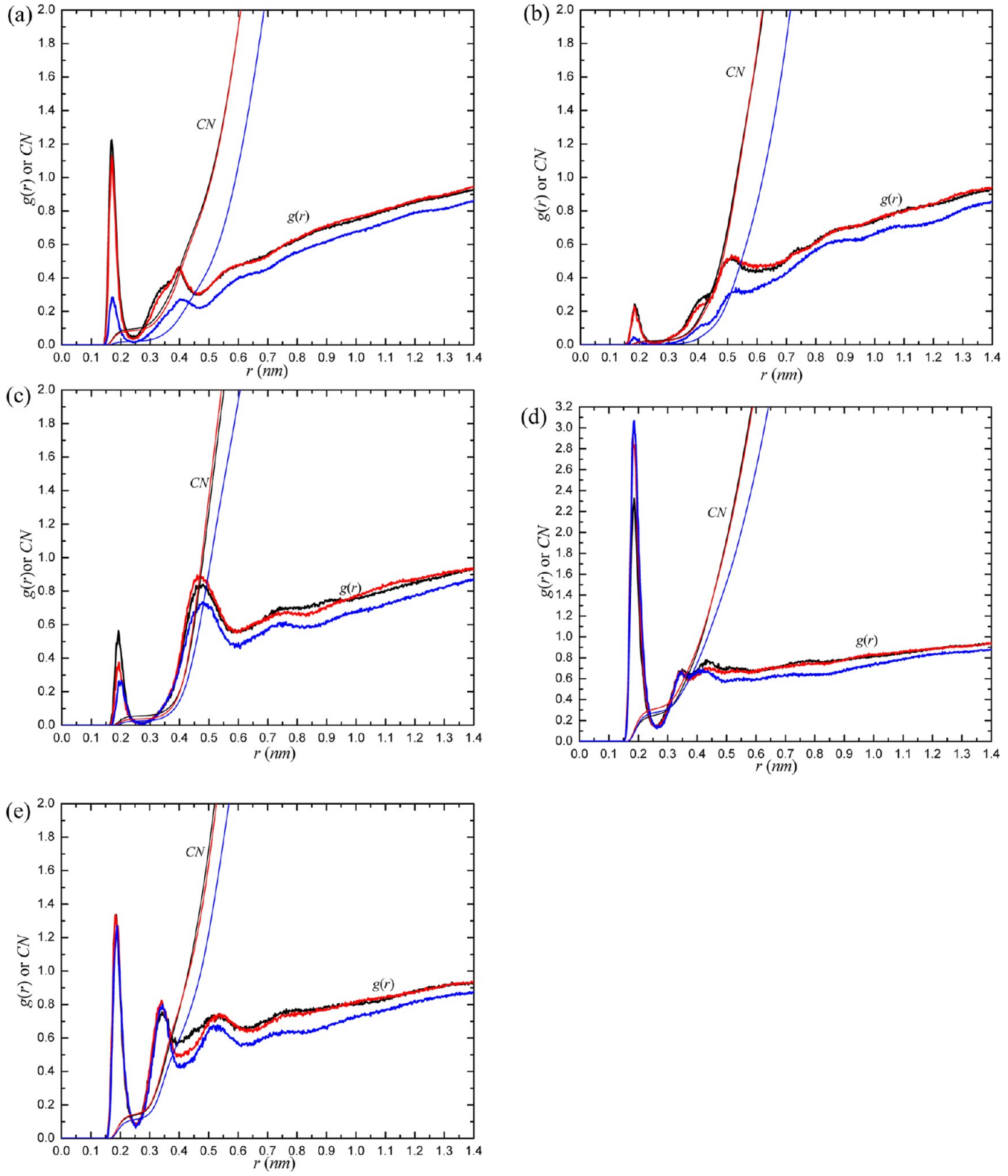

Figure 17. RDFs and CNs of (a) (OS_{HEPES}–$HO_{alcohol}$), (b) (HN_{HEPES}–$OH_{alcohol}$), (c) (N_{HEPES}–$HO_{alcohol}$), (d) (OH_{HEPES}–$HO_{alcohol}$), and (e) (HO_{HEPES}–$OH_{alcohol}$) obtained from MD simulations of $S_{1\text{-propanol}}$ (black), $S_{2\text{-propanol}}$ (red), and $S_{tert\text{-butanol}}$ (blue) systems. $S_{1\text{-propanol}}$ = HEPES + water + 1-propanol system; $S_{2\text{-propanol}}$ = HEPES + water + 2-propanol system, and $S_{tert\text{-butanol}}$ = HEPES + water + *tert*-butanol system.

10 shows the electrostatic potential (ESP) of HEPES in water which mapped on an electron-density isosurface. The ESP map can be used to predict the possible interaction sites of HEPES molecule with solvent. The sulfonic group and the oxygen atom of the hydroxyl group possess a negative ESP, and this explains the high affinity of these groups to water molecules. Thus, the high water affinity of HEPES is mainly due to electrostatic interaction, since it is generally accepted that HBs are primarily electrostatic interactions in origin.[87] The electrostatic (Coulomb) and the van der Waals (Lennard-Jones) interaction

dx.doi.org/10.1021/jp305516g | J. Phys. Chem. B 2013, 117, 563−582

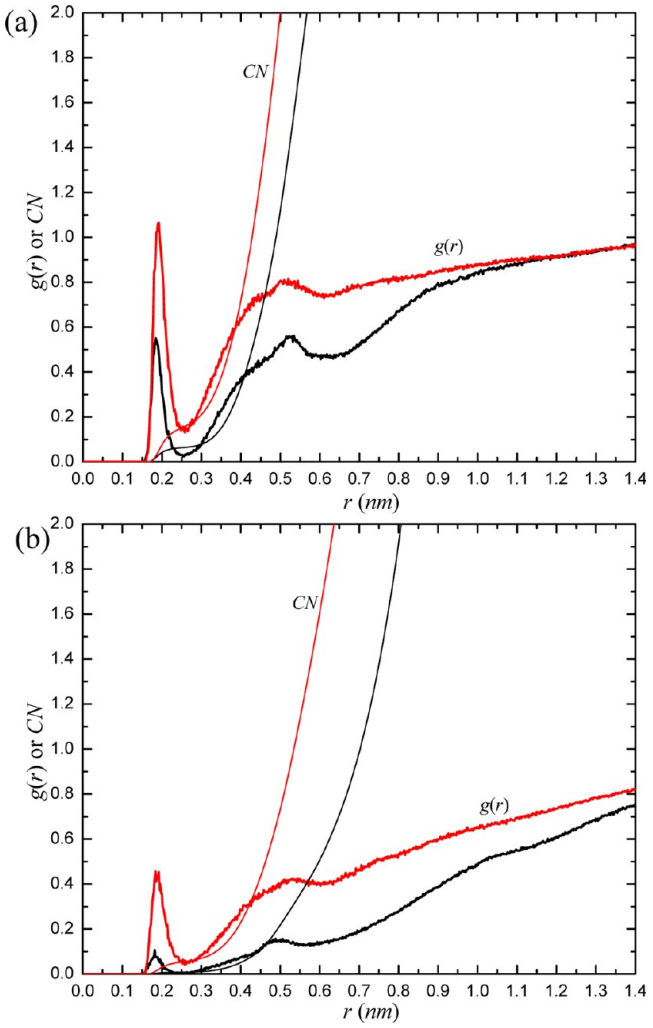

Figure 18. RDFs and CNs of (black) (HN_{HEPES}–$N_{acetonitrile}$)/(HN_{HEPES}–$O_{acetone}$) and (red) (HO_{HEPES}–$N_{acetonitrile}$)/(HO_{HEPES}–$O_{acetone}$) obtained from MD simulations of (a) $S_{acetonitrile}$ and (b) $S_{acetone}$ systems. $S_{acetonitrile}$ = HEPES + water + acetonitrile system and $S_{acetone}$ = HEPES + water + acetone system.

energies obtained from the MD simulation systems (M1–M12) are summarized in Table 7. The electrostatic energy is more expressed and the van der Waals interaction is destabilizing, between HEPES and water molecules. For instance, the electrostatic and the van der Waals interactions between a HEPES molecule and water molecules (M1) are −689 and 25.9 kJ·mol^{-1}, respectively. The van der Waals interactions then gradually increased with increasing the THF concentrations (M4 to M11) and reached 364.7 kJ·mol^{-1} at M11. The electrostatic interactions between HEPES and water molecules are much larger than both electrostatic and van der Waals interactions between HEPES and THF molecules. The nonbonding interaction values between HEPES molecules themselves are also negative and increased with the addition of THF and reached −1980 and −101.7 kJ·mol^{-1} for the electrostatic and van der Waals interactions, respectively. Thus, the preferential hydration of HEPES molecules is further strengthened by the analysis of the nonbonding energies.

Figure 11 shows a snapshot taken from MD simulation of HEPES in pure THF system (M12). Interestingly, we can see that all 10 HEPES molecules are entirely aggregated in pure THF. This indicates that HEPES is insoluble in pure THF, which agrees with the experimental results (phase diagrams). By investigating the HBs formation between HEPES ZI molecules themselves (Figure 11), it can be concluded that the oxygen atoms of the sulfonic group are H-bounded with the hydrogen atoms of the hydroxyl and the amine groups. Snapshots were also obtained from MD simulations for M4 to M8 systems (L region) and shown in Figure 12. Moving from M4 to M8 composition, the THF clusters are formed especially at high THF concentrations (M6 to M8). In fact, the cluster behavior of the studied organic solvents is known to exist in aqueous solutions. Takamuku and co-workers[88] have studied the mixing states of the aqueous mixtures of cyclic ethers, THF, 1,3-dioxane, and 1,4-dioxane, from the microscopic to mesoscopic levels. The microheterogeneity is in the sequence of THF > 1,3-dioxane ≫1,4-dioxane. The short distance between oxygen atoms makes 1,3-dioxane molecule less suitable to fit into the hydrogen-bonded network of water than the 1,4-dioxane molecule.[88] The mixing state of 1,3-dioxolane is probably similar to that of 1,3-dioxane; i.e., two oxygen atoms are positioned at a meta site. Numerous small-angle X-ray scattering (SAXS) analysis results are available for aqueous solutions of 1-propanol, 2-propanol, and *tert*-butanol.[89−94] The aggregation behavior was observed from the SAXS studies for these aqueous systems. Hayashi and co-workers[93] found that 1-propanol molecules have a stronger tendency to gather in the aqua solution than *tert*-butanol molecules. Moreover, 2-propanol is more miscible with water and the clusters in 2-propanol–water solution are smaller than those in the 1-propanol–water solution; that is, the heterogeneity in the 2-propanol solution is less than that in the 1-propanol solution.[93] It was found recently that acetonitrile molecules form three-dimensional clusters and these clusters are surrounded by water molecules through hydrogen-bonding and dipole–dipole interactions.[95] Snapshots were also taken from MD simulations for M9 to M11 systems (2L region) and given in Figure 13. Amazingly, inside the phase separation regions (2L), the THF clusters are forced out from the water network to form a new liquid phase and the water clusters were evolved around the HEPES molecules. Thus, water-rich and THF-rich phases are splitting from the mixture of M9 to M11. The evolution in the phase separation (i.e., M9) was evaluated by looking at selected snapshots (Figures 14), and quantitatively achieved by monitoring the potential energy (U) of the system as function of time (Figures 15). The phase separation was rapid and the configurations converted into two-liquid phase in less than 2 ns. Similar behavior has been observed previously in water–chloroform (less than 0.5 ns)[96] and water–oil mixtures (less than 1 ns);[97] and in other MD simulation mixtures such as ionic liquids/water,[98,99] the convergence was very slow (typically, in greater than 20 ns).

From our MD simulation results of HEPES in water, many water molecules are found in direct contact with HEPES through hydrogen bonds. This is due to the excessive strong proton acceptors of the sulfonic group and free nitrogen atom, as well as proton donors of the amine group and the hydroxyl group; on average, 11.65 H-bonds are observed between HEPES and water molecules. On the other hand, HEPES shows low affinity to H-bonds formation with THF molecules in pure THF, on average 0.174, via the proton donor sites of HEPES molecule. This value even decreases in the presence of water molecules. The electrostatic interactions due to the zwitterion nature of HEPES buffer and the van der Waals interactions of HEPES with water molecules are found to be

dx.doi.org/10.1021/jp305516g | J. Phys. Chem. B 2013, 117, 563–582

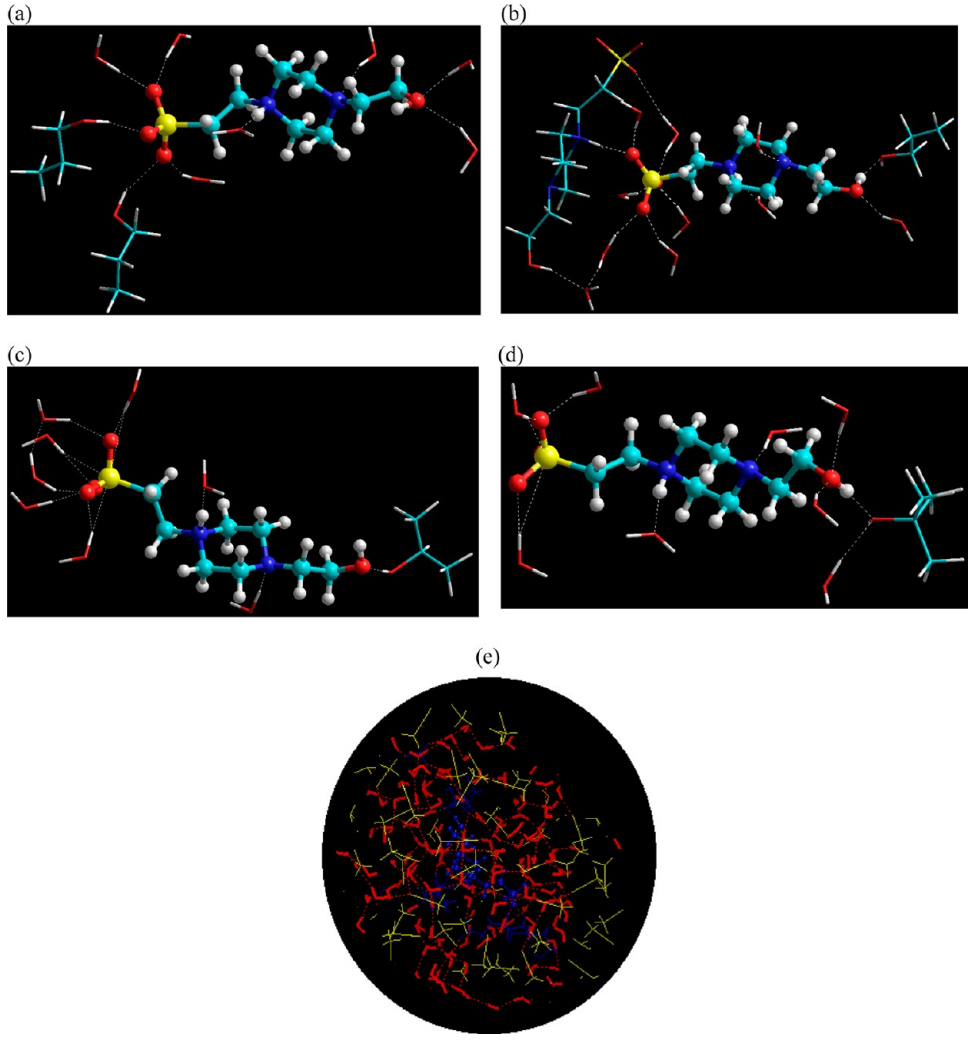

Figure 19. MD snapshots showing the H-bonds between HEPES and 1-propanol (a,b), 2-propanol (c), and *tert*-butanol (d), obtained from MD simulations on $S_{alcohol}$ systems at 15 ns. (e) MD snapshot showing the HBs between acetonitrile and water shells bounded to HEPES molecules, obtained from MD simulation on the $S_{acetonitrile}$ system at 15 ns.

much greater than those with THF molecules. The THF clusters were formed in the mixture due to the weak THF−water interactions in the presence of HEPES, and gradually growing with the addition of THF molecules and forming a nanoscopic liquid phase above the solvated buffer. However, when looking at the other organic solvents, there are significant differences in their hydrophobicity/hydrophilicity characters, and then one has to ask whether HEPES in mixtures of these solvents with water can behave the same as in THF−water mixtures. In order to answer this question, we performed MD simulations for HEPES in aqueous mixtures containing 1,3-dioxolane, 1,4-dioxane, 1-propanol, 2-propanol, *tert*-butanol, acetonitrile, or acetone, respectively. The simulation box for each system contains 10 HEPES, 629 water, and 361 organic solvent molecules which similar to M10 composition of HEPES + water + THF system and these compositions are located inside the phase separation region (2L). The $\langle N_{HB} \rangle$ values as well as electrostatic and van der Waals energies between the different pairs of the mixtures are reported in Tables 8 and 9, respectively. Once again, we see here the high affinity of HEPES for water and its insignificant interactions toward the organic solvents. The water molecules also formed extensive HBs with the hydrophilic atoms on the HEPES molecules; i.e., $\langle N_{HB} \rangle$ values are greater than 9.7. The $\langle N_{HB} \rangle$ values between the latter and organic solvents 1,3-dioxolane, 1,4-dioxane, and acetone are very small, $\leq$0.057. From Table 8, we also see that $\langle N_{HB} \rangle$ values between HEPES and acetonitrile/aliphatic alcohols are higher than those of acetone or the cyclic ethers. The same trend is also observed between the organic solvents and water. This is expected due to the high polarity of acetonitrile and the hydrophilicity of the aliphatic alcohols. Further, it appears from the tabulated values that the interactions between acetonitrile/alcohols with water rupture the HBs within the water network greater than that resulting from the other organic solvent−water interactions. The dehydration of HEPES in all systems is almost the same as it appeared from the $\langle N_{HB} \rangle$ values between HEPES molecules themselves. The electrostatic and the Lennard-Jones energies between the pairs HEPES−water, HEPES−organic solvent, and organic solvent−water (Table 9) followed the same behavior as obtained from the $\langle N_{HB} \rangle$ results.

The peak positions of HEPES's atomic sites−water RDFs in presence of these organic solvents are similar to those in THF−water mixtures; only their relative intensities are changed, and the corresponding CN curves are given in Figures S1−S3 in the Supporting Information. It is interesting here to explore the

dx.doi.org/10.1021/jp305516g | *J. Phys. Chem. B* 2013, 117, 563−582

RDFs and CN for the HEPES's atomic sites with the organic solvents. Figure 16 shows the ($HO_{HEPES}\cdots O_{1,3\text{-dioxolane}/1,4\text{-dioxane}}$) and ($HN_{HEPES}\cdots O_{1,3\text{-dioxolane}/1,4\text{-dioxane}}$) RDFs as well as their respective CN curves, but the CNs for latter are not shown because it was not possible to identify the first peak. This figure shows that the interactions between HEPES and cyclic ethers are weak, and mainly through the ($HO_{HEPES}\cdots O_{1,3\text{-dioxolane}/1,4\text{-dioxane}}$) type, a small peak at 0.18 nm with low intensity has been observed and the first-shell CN value for ($HO_{HEPES}\cdots O_{1,3\text{-dioxolane}}$) is greater than that of ($HO_{HEPES}\cdots O_{1,4\text{-dioxane}}$). The ($OS_{HEPES}\cdots HO_{alcohol}$), ($HN_{HEPES}\cdots OH_{alcohol}$), ($N_{HEPES}\cdots HO_{alcohol}$), ($OH_{HEPES}\cdots HO_{alcohol}$), and ($HO_{HEPES}\cdots OH_{alcohol}$) are displayed in Figure 17. This figure tells us that, among the HEPES's atomic sites, the hydroxyl group mostly interacts, especially via the oxygen atom, with alcohol's hydroxyl group and then the sulfonic group. The protonated amine's hydrogen atom and the nitrogen atom nearby the hydroxyl group are rarely interacting with the alcohol's hydroxyl group. Figure 18 displays ($HO_{HEPES}\cdots N_{actonitrile}$)/($O_{acetone}$) and ($HN_{HEPES}\cdots N_{actonitrile}$)/($O_{acetone}$) RDFs and the respective CN curves, and this result shows that the former interaction is more dominant. The current simulations with a composition inside the 2L region of the previously mentioned phase separation systems reveal that the organic solvents are squeezed out from the mixture and form a new phase; the snapshots shown in Figures S4–S6 in the Supporting Information. In case of the HEPES + water + cyclic ether/acetone systems, clear distinct nanoscopic phases separated by an interface were obtained, but in the acetone case, some water molecules were trapped in inside the acetone phase and vice versa. However, in the case of alcohols, water/HEPES-rich and alcohol-rich domains appear due to interactions between HEPES and alcohol (Figure 19a–d). The snapshot displayed in Figure 19e shows that acetonitrile molecules form HBs with the water shells bounded to HEPES molecules.

CONCLUSIONS

Herein we have presented a new liquid–liquid phase splitting phenomenon, buffering-out, by addition of organic solute (buffer, HEPES) into aqueous solutions of water-miscible organic solvent (1-propanol, 2-propanol, *tert*-butanol, THF, 1,3-dioxolane, 1,4-dioxane, acetonitrile, or acetone). The binodal data were fitted to an empirical equation relating the concentrations of organic solvent and buffer, and the coefficients were estimated. The formation of two-liquid-phase phenomena was visualized with different disperse dyestuffs. Furthermore, with the aid of MD simulations, we thoroughly examined the intermolecular interactions among HEPES buffer, water, and the organic solvents. The MD simulations have shown that HEPES buffer is preferentially solvated by water even at high organic solvent concentrations, and rarely interacts with the organic solvent. The water clusters and the organic solvent clusters were formed in the mixture, in which the former clusters were evolved around the HEPES molecules, with the latter clusters gradually growing with the addition of more organic solvent molecules until forming a macroscopic liquid phase above the solvated buffer. The new two-liquid phase splitting behavior may be helpful in the recovery of the organic solvents from the spent aqueous solutions, especially from the azeotropic solutions, and may find potential applications in the separation of chemicals having substantially different solubilities in water and in the organic solvent.

ASSOCIATED CONTENT

Supporting Information

Tables of densities and solubilities; scheme showing labels and symbols of HEPES atoms; figures showing RDFs for the interactions of HEPES's atomic sites, CNs for the interactions of HEPES's atomic sites, and snapshots obtained from MD simulations. This material is available free of charge via the Internet at http://pubs.acs.org.

AUTHOR INFORMATION

Corresponding Author

*Tel.: +886-2-2737-6626. Fax: +886-2-2737-6644. E-mail: mjlee@mail.ntust.edu.tw.

Notes

The authors declare no competing financial interest.

ACKNOWLEDGMENTS

The authors gratefully acknowledge the financial support from National Taiwan University of Science and Technology and the National Science Council, Taiwan, through NSC99-2811-E-011-023 and NSC99-2221-E011-079-MY3. M.T. acknowledges postdoc fellowship through this grant. The authors thank Dr. Ho-mu Lin for valuable discussions and acknowledge the use of the NTUST High Performance Computing Facility for computer time and systems support. We sincerely thank the reviewers for their comments and suggestions.

REFERENCES

(1) Gu, Y.; Shih, P.-H. *Enzyme Microb. Technol.* **2004**, *35*, 592–597.
(2) Gu, T.; Zhang, L. *Chem. Eng. Commun.* **2007**, *194*, 828–834.
(3) Salabat, A. *Fluid Phase Equilib.* **2007**, *257*, 1–5.
(4) Le, Q.; Shong, L.; Shi, Y. *Sep. Purif. Technol.* **2001**, *24*, 85–91.
(5) Liang, R.; Wang, Z.; Xu, J.-H.; Li, W.; Qi, H. *Sep. Purif. Technol.* **2009**, *66*, 248–256.
(6) Lehninger, A. L. *Principles of Biochemistry*; Worth: New York, 1982.
(7) Frankforter, G. B.; Frary, E. C. *Phys. Chem.* **1913**, *17*, 402–473.
(8) Frankforter, G. B.; Cohen, L. *J. Am. Chem. Soc.* **1914**, *36*, 1103–1134.
(9) Ginnings, P. M.; Chen, Z. T. *J. Am. Chem. Soc.* **1931**, *53*, 3765–3769.
(10) Ginnings, P. M. *J. Am. Chem. Soc.* **1930**, *52*, 2282–2286.
(11) Kobe, K. A.; Stone, J. P. *J. Phys. Chem.* **1940**, *44*, 629–633.
(12) Sada, E.; Morisue, T.; Miyahara, K. *J. Chem. Eng. Data* **1975**, *20*, 283–287.
(13) Legget, D. C.; Jenkins, T. F.; Mayares, P. H. *Anal. Chem.* **1990**, *62*, 1355–1356.
(14) Warren, K. W. *Reduction of Corrosion through Improvements in Desalting*; Benelux Refinery Symposium: Lanaken, Belgium, 1995.
(15) Leinonen, H. *Corrosion* **1996**, *52*, 337–346.
(16) Gu, T.; Gu, Y.; Zheng, Y.; Wiehl, P. E.; Kochick, J. *J. Sep. Technol.* **1994**, *4*, 258–260.
(17) Tabata, M.; Kumamoto, M.; Nishimoto. *J. Anal. Sci.* **1994**, *10*, 383–388.
(18) Tabata, M.; Kumamoto, M.; Nishimoto. *J. Anal. Chem.* **1996**, *68*, 758–762.
(19) Chung, N. H.; Nishimoto, J.; Kato, O.; Tabata, M. *Anal. Chim. Acta* **2003**, *477*, 243–249.
(20) Wang, B.; Feng, H.; Ezeji, T.; Blaschek, H. *Chem. Eng. Technol.* **2008**, *31*, 1869–1874.
(21) Albetsson, P.-A. *Partition of Cell Particles and Macromolecules*; Wiley-Interscience: New York, 1986.

(22) Beijernick, M. W. *Zentralbl. Bakteriol., Parasitenkunde Infektioskrankheiten* **1896**, *22*, 699−701.
(23) Albertsson, P. A. *Nature* **1956**, *177*, 771−774.
(24) Köhler, K.; Ljungquist, C.; Kondo, A.; Veide, A.; Nilsson, B. *Nature* **1991**, *9*, 642−646.
(25) Taha, M.; Lee, M. J. *Biochem. Eng. J.* **2009**, *46*, 334−344.
(26) Taha, M.; Lee, M. J. *J. Chem. Thermodyn.* **2011**, *43*, 1723−1730.
(27) Taha, M.; Lee, M. J. *J. Chem. Eng. Data* **2011**, *56*, 4436−4443.
(28) Taha, M.; Teng, H. L.; Lee, M. J. *J. Chem. Thermodyn.* **2012**, *47*, 154−161.
(29) Taha, M.; Teng, H. L.; Lee, M. J. *J. Chem. Thermodyn.* **2012**, *54*, 134−141.
(30) Taha, M.; Gupta, B. S.; Khoiroh, I.; Lee, M. J. *Macromolecules* **2011**, *44*, 8575−8589.
(31) Luo, S.; Pal, D.; Shah, S. J.; Kwatra, D.; Paturi, K. D.; Mitra, A. K. *Mol. Pharm.* **2010**, *7*, 412−420.
(32) Chen, R.; Wu, J.; Li, H.; Cheng, G.; Lu, Z.; Che, C.-M. *Rare Met.* **2010**, *29*, 180−186.
(33) Xie, J.; Lee, J. Y.; Wang, D. I. C. *Chem. Mater.* **2007**, *19*, 2823−2830.
(34) Serizawa, T.; Hirai, Y.; Aizawa, M. *Langmuir* **2009**, *25*, 12229−12234.
(35) Sun, R. W.-Y.; Chen, R.; Chung, N. P.-Y.; Ho, C.-M.; Lin, C.-L. S.; Che, C.-M. *Chem. Commun.* **2005**, *28*, 5059−5061.
(36) So, M. H.; Ho, C. M.; Chen, R.; Che, C.-M. *Chem. Asian J.* **2010**, *5*, 1322−1331.
(37) Habib, A.; Tabata, M.; Wu, Y. G. *Bull. Chem. Soc. Jpn.* **2005**, *78*, 262−269.
(38) Li, H.; Lu, Z.; Wu, J.; Yu, H.; Yu, X.; Chen, R. *Mater. Lett.* **2010**, *64*, 1939−1942.
(39) Li, H.; Lu, Z.; Li, Q.; So, M.-H.; Che, C. M.; Chen, R. *Chem. Asian J.* **2011**, *6*, 2320−2331.
(40) Helfrich, M. R.; El-Kouedi, M.; Etherton, M. R.; Keating, C. D. *Langmuir* **2005**, *21*, 8478−8486.
(41) Dinsmore, D.; Hsu, M. F.; Nikolaides, M. G.; Marquez, M.; Bauch, A. R.; Weitz, D. A. *Science* **2002**, *298*, 1006−1009.
(42) Zheng, L.; Li, J. *J. Phys. Chem. B* **2005**, *109*, 1108−112.
(43) Silver, B. R.; Fülöp, V.; Unwin, P. R. *New J. Chem.* **2011**, *35*, 602−606.
(44) Lindahl, E.; Hess, B.; van der Spoel, D. *J. Mol. Model.* **2001**, *7*, 306−17.
(45) van der Spoel, D.; Lindahl, E.; Hess, B.; Groenhof, G.; Mark, A. E.; Berendsen, H. J. C. *J. Comput. Chem.* **2005**, *26*, 1701−1718.
(46) Berendsen, H. J. C.; Grigera, J. R.; Straatsma, T. P. J. *Phys.Chem.* **1987**, *91*, 6269−6271.
(47) Lee, C.; Yang, W.; Parr, R. G. *Phys. Rev. B* **1988**, *37*, 785−789.
(48) Becke, A. D. *J. Chem. Phys.* **1993**, *98*, 5648−5652.
(49) Stephens, P. J.; Devlin, F. J.; Chabalowski, C. F.; Frisch, M. J. *J. Phys. Chem.* **1994**, *98*, 11623−11627.
(50) Vosko, L. W. S. H.; Nusair, M. *Can. J. Phys.* **1980**, *58*, 1200−1211.
(51) Frisch, M. J.; Trucks, G. W.; Schlegel, H. B.; Scuseria, G. E.; Robb, M. A.; Cheeseman, J. R.; Scalmani, G.; Barone, V.; Mennucci, B.; Petersson, G. A.; et al. *Gaussian 09, revision A.02*; Gaussian, Inc.: Wallingford, CT, 2009.
(52) Jorgensen, W. L.; Maxwell, D. S.; Tirado-Rives, J. *J. Am. Chem. Soc.* **1996**, *118*, 11225−11236.
(53) Ribeiro, A. A. S. T.; Horta, B. A. C.; de Alencastro, R. B. *J. Braz. Chem. Soc.* **2008**, *19*, 1433−1435.
(54) Caleman, C.; van Maaren, P. J.; Hong, M.; Hub, J. S.; Costa, L. T.; van der Spoel, D. *J. Chem. Theory Comput.* **2012**, *8*, 61−74.
(55) Nagy, P. I.; Volgyi, G.; Takacs-Novak, K. *J. Phys. Chem. B* **2008**, *112*, 2085−2094.
(56) Darden, T.; York, D.; Pedersen, L. *J. Chem. Phys.* **1993**, *98*, 10089−10092.
(57) Hockney, R. W.; Goel, S. P. J. *J. Comput. Phys.* **1974**, *14*, 148−158.
(58) Nosé, S. *Mol. Phys.* **1984**, *52*, 255. Hoover, W. G. *Phys. Rev .A* **1985**, *31*, 1695−1697.
(59) Parrinello, M.; Rahman, A. *J. Appl. Phys.* **1981**, *52*, 7182−7190.
(60) Humphrey, W.; Dalke, A.; Schulten, K. *J. Mol. Graph.* **1996**, *14*, 33−38.
(61) van der Spoel, D.; van Maaren, P. J.; Larsson, P.; Tîmneanu. *J. Phys. Chem. B* **2006**, *110*, 4393−4398.
(62) Reichardt, C. *Solvents and Solvent Effects in Organic Chemistry*; Wiley-VCH: Weinheim, Germany, 2003.
(63) Pimentel, G. C.; McClellan, A. L. *The Hydrogen Bond*; Freeman Co.: New York, 1960.
(64) Debye, P.; MacAulay, J. *Z. Phys. Chem.* **1925**, *26*, 22−29.
(65) McDevit, W. F.; Long, F. A. *Chem. Rev.* **1952**, *51*, 119−169.
(66) Aveyard, R.; Heselden, R. *J. Chem. Soc., Faraday Trans. 1* **1975**, *71*, 312−321.
(67) Fromon, M.; Treiner, C. J. *J. Chem. Soc., Faraday Trans. 1* **1979**, *75*, 1837−1848.
(68) Conway, B. E. *Pure Appl. Chem.* **1985**, *57*, 263−272.
(69) Haugen, G. R.; Friedman, H. L. *J. Phys. Chem.* **1963**, *67*, 1757−1761.
(70) Krishnan, C. V.; Friedman, H. L. *J. Solution Chem.* **1974**, *9*, 727−744.
(71) Hall, D. G. *Trans. Faraday Soc.* **1971**, *67*, 2516−2424.
(72) Misawa, M.; Yoshida, K.; Maruyama, K.; Munemura, H.; Hosokawa, Y. *J. Phys. Chem. Solids* **1999**, *60*, 1301−1306.
(73) Yoshida, K.; Misawa, M.; Maruyama, K.; Imai, M.; Furusaka, M. *J. Chem. Phys.* **2000**, *113*, 2343−2348.
(74) Takamuku, T.; Yamaguchi, A.; Matsuo, D.; Tabata, M.; Yamaguchi, T.; Otomo, T.; Adachi, T. *J. Phys. Chem. B* **2001**, *105*, 10101−10110.
(75) Takamuku, T.; Yamaguchi, A.; Matsuo, D.; Tabata, M.; Kumamoto, M.; Nishimoto, J.; Yoshida, K.; Yamaguchi, T.; Nagao, M.; Otomo, T.; Adachi, T. *J. Phys. Chem. B* **2001**, *105*, 6236−6245.
(76) Takamuku, T.; Noguchi, Y.; Yoshikawa, E.; Kawaguchi, T.; Matsugami, M.; Otomo, T. *J. Mol. Liq.* **2007**, *131*−*132*, 131−138.
(77) Takamuku, T.; Shimomura, T.; Tachikawa, M.; Kanzaki, R. *Phys. Chem. Chem. Phys.* **2011**, *13*, 11222−11232.
(78) Mendez-Morales, T.; Carrete, J.; Cabeza, O.; Gallego, L. J.; Varela, L. M. *J. Phys. Chem. B* **2011**, *115*, 11170−11182.
(79) Mendez-Morales, T.; Carrete, J.; García, M.; Cabeza, O.; Gallego, L. J.; Varela, L. M. *J. Phys. Chem. B.* **2011**, *115*, 15313−15322.
(80) Kirkwood, J. G. *J. Chem. Phys.* **1934**, *2*, 351−361.
(81) Neuberger, A. *Proc. Roy. Soc. London A* **1937**, *158*, 68−96.
(82) Robinson, R. A.; Stokes, R. H. *Electrolyte Solutions*; Dover: Mineola, NY, 2002.
(83) Roy, R. N.; Robinson, R. A.; Bates, R. G. *J. Am. Chem. Soc.* **1973**, *95*, 8231−8235.
(84) Cecchi, T.; Cecchi, P. *Chromatographia* **2002**, *55*, 279−282.
(85) Cecchi, T.; Pucciarelli, F.; Passamonti, P. *Analyst* **2004**, *129*, 1037−1046.
(86) Marcus, Y. *J. Mol. Liq.* **2006**, *123*, 8−13.
(87) Jorgensen, W. L.; Maxwell, D. S.; Tirado-Rives, J. *J. Am. Chem. Soc.* **1996**, *118*, 11225−11236.
(88) Takamuku, T.; Nakamizo, A.; Tabata, M.; Yoshida, K.; Yamaguchi, T.; Otomo, T. *J. Mol. Liq.* **2003**, *103*−*104*, 143−159.
(89) Koga, Y. *Chem. Phys. Lett.* **1984**, *111*, 176−180.
(90) Nishikawa, K. *Chem. Phys. Lett.* **1986**, *132*, 50−53.
(91) Nishikawa, K.; Kodera, Y.; Iijima, T. *J. Phys. Chem.* **1987**, *91*, 3694−3699.
(92) Nishikawa, K.; Hayashi, H.; Iijima, T. *J. Phys. Chem.* **1989**, *93*, 6559−6565.
(93) Hayashi, H.; Nishikawa, K.; Iijima, T. *J. Phys. Chem.* **1990**, *94*, 8334−8338.
(94) Hayashi, H.; Udagawa, Y. *Bull. Chem. Soc. Jpn.* **1992**, *65*, 155−159.
(95) Takamuku, T.; Tabata, M.; Yamaguchi, A.; Nishimoto, J.; Jumamoto, M.; Wakita, H.; Yamaguchi, T. *J. Phys. Chem. B* **1998**, *102*, 8880−8888.
(96) Muzet, N.; Engler, E.; Wipff, G. J. *Phys. Chem. B* **1998**, *102*, 10772−10788.

(97) Baaden, M.; Schurhammer, R.; Wipff, G. *J. Phys. Chem. B* **2002**, *106*, 434−441.
(98) Chaumont, A.; Schurhammer, R.; Wipff, G. J. *Phys. Chem. B* **2005**, *109*, 18964−18973.
(99) Sieffert, N.; Wipff, G. *J. Phys. Chem. B* **2006**, *110*, 13076−13085.